On the strange case of divalent ions intercalation in V2O5

Roberta Verrelli, Ashley Philip Black, Chanachai Pattanathummasid, Deyana S. Tchitchekova, Alexandre Ponrouch, Judith Oró-Solé, Carlos Frontera, Fanny Bardé, Patrick Rozier, Rosa Palacín

On the strange case of divalent ions intercalation in V_2O_5

R. Verrelli[a,1], A.P. Black[a,1], C. Pattanathummasid[a,b], D.S. Tchitchekova[a], A. Ponrouch[a],
J. Oró-Solé[a], C. Frontera[a], F. Bardé[c], P. Rozier[b], M.R. Palacín[a,*]

[a] Institut de Ciència de Materials de Barcelona (ICMAB-CSIC), Campus UAB, E-08193, Bellaterra, Catalonia, Spain
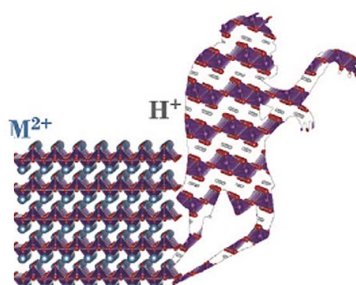[b] Université Paul Sabatier, CIRIMAT, UMR CNRS 5085, 118 Route de Narbonne, 31062, Toulouse Cedex, France
[c] Toyota Motor Europe, Research & Development 2, Advanced Material Research, Technical Centre, Hoge Wei 33 B, B-1930, Zaventem, Belgium

GRAPHICAL ABSTRACT

ABSTRACT

Vanadium pentoxide has been investigated for multivalent ion battery technologies but the structural characterization of inserted phases is poor, and conflicting reports exist in the literature. This study presents a critical overview of controversial aspects related to Mg and Ca insertion in α-V_2O_5 under diverse conditions by combined electrochemical and ex-situ XRD experiments. Galvanostatic tests are carried out in dry and wet alkyl carbonate-based electrolytes at RT and 100 °C. The formation of protonated phases with negligible divalent ion content if any is evidenced by Rietveld refinements of the XRD data, unambiguously dismissing the presence of AV_2O_5 (A: Mg, Ca) as electrochemical reduction products. Furthermore, thermal instability of V_2O_5 at 100 °C in alkyl carbonate solvents is demonstrated by XRD and TEM analysis and the formation of an orthorhombic phase with increased a parameter, most likely due to degradation favored by both water and temperature, is observed for both Mg and Ca. In order to assess the feasibility of the reverse reaction, fully intercalated AV_2O_5 (A = Ca, Mg) phases were also prepared by solid state reaction and oxidation attempted both electrochemically and chemically without evidence of any significant amount of Mg^{2+} or Ca^{2+} extraction, further corroborating the sluggish diffusion kinetics of divalent cations in α-V_2O_5.

1. Introduction

Development of new battery technologies involving multivalent

metal anodes (e.g. Mg, Ca, Al) has recently re attracted the interest of the scientific community, as these rely on abundant, inexpensive and nontoxic metals and hold promise of very high energy densities [1].

Amongst them, Mg batteries have deserved the most attention, with proof of concept being given as early as 2000 using Chevrel phases as positive electrode material [2], despite commercialization being still elusive due to diverse fundamental bottlenecks [3,4]. On the other hand, the recent reports on the feasibility of Ca plating and stripping [5,6] opened the quest for materials reversibly inserting and extracting Ca^{2+} that could be used as positive electrode to achieve proof of con cept of a full Ca based battery. Besides the exploration of new materials [7 9], revisiting traditional layered intercalation hosts appear as a very useful tool to gain further insight into the fundamentals of divalent ion intercalation [10]. Indeed, even if the know how gained in the devel opment of the Li ion battery technology is precious to accelerate ad vances in alternative electrochemical energy storage systems, it cannot be directly translated to divalent chemistries, as many of the aspects taken for granted (reliability of reference electrodes, absence of side reactions etc) do not hold when moving to Mg or Ca based chemistries [11] and the use of a wide spectrum of characterization tools is com pulsory [12 16] to avoid biased interpretation of results. The case of V_2O_5 is especially intriguing. Despite the expected low multivalent ion mobility in oxide hosts, it seems at first sight well established that it does intercalate both Ca^{2+} and Mg^{2+} ions. Nonetheless, the inter pretation of some observed trends deserves further attention and some relevant controversies emerge from the available literature [16]. On one hand the addition of water to magnesium electrolytes as "shielding" agent was suggested to promote intercalation of Mg^{2+} ions but alter native effects of water or hydronium ions have not been unambiguously interpreted [17,18]. On the other hand, elucidation of the intercalated $A_xV_2O_5$ crystal structure remains elusive, despite some changes in the XRD patterns of pristine orthorhombic V_2O_5 observed after intercala tion, which differ from one study to another (see next section).

Energy barriers for multivalent (MV) ion migration and the V_2O_5 MV ion phase diagram have been recently computed [19 21], which should contribute to clarify the situation. According to the first prin ciples calculations performed by Sai Gautam et al. [20], the intercala tion of Mg^{2+} in α V_2O_5 under equilibrium conditions should evolve through a two phase reaction, with nucleation of δ $Mg_xV_2O_5$ (0 < x < 1) from demagnesiated α V_2O_5, the absence of experimental evidence being attributed to hindered kinetics. Instead, the formation of the metastable ϵ phase (with ordering at x = 0.5 resulting in a voltage drop on the electrochemical profile) is more consistent with experi ments, since it does not require structural rearrangement of the host structure. Alternative studies [22] predict a phase transformation from α to δ polymorph while discussing a possible competition with Mg^{2+} ion diffusion (with estimated Mg hopping barriers of 1.26 and 0.81 eV for the α and δ phase, respectively). The α and δ V_2O_5 polymorphs differ in the stacking of the layers along the a direction, which results in a different coordination environment for the intercalation site (see Fig. 1) . Since Mg^{2+} migration is predicted to be faster and en ergetically more favorable in the δ polymorph, the deintercalation of magnesium from δ MgV_2O_5, which can be directly synthesized by solid

state reaction [23], is suggested as a viable strategy to foster the Mg^{2+} mobility and achieve good electrochemical performance [20].

In the case of Ca^{2+} ions, the available DFT studies [21,24] predict migration barriers of about 1.7 1.9 eV in α V_2O_5 with an average vol tage of about 3.2 V vs Ca^{2+}/Ca. In contrast, the migration barrier in the δ V_2O_5 phase is calculated to be much lower (0.2 eV). However, this polymorph is not known: CaV_2O_5 prepared by solid state reaction is not isostructural with δ MgV_2O_5, but rather exhibits the α structure, which enables a more suitable coordination for the larger Ca^{2+} ion [25].

Aiming to move further steps towards the understanding of the critical aspects related to MV ion intercalation into V_2O_5, we have in vestigated the electrochemical behavior of orthorhombic α V_2O_5 both in Mg and Ca cells, in dry and wet alkyl carbonate based electrolytes, with a critical focus on the insertion driven structural changes of the active phase as observed by ex situ X ray diffraction.

Approaching the subject from the opposite side, AV_2O_5 phases (A: Mg, Ca) were prepared by solid state synthesis and their oxidation was attempted chemically and electrochemically. This approach, to the best of our knowledge here originally explored, addresses the open ques tions on the possible structural transformation of fully intercalated AV_2O_5 phases into V_2O_5 (and vice versa), to date not yet thoroughly clarified. The results achieved in this study underpin the importance of a rigorous methodology combining electrochemical and alternative characterization techniques to unambiguously assess MV ion inter calation.

2. Overview of a controversial background

Orthorhombic α V_2O_5 is built up by layers of alternating edge and corner sharing VO_5 square pyramids linked together through Van der Waals interactions (S.G. *Pmmn*). It holds potential for multielectron intercalation reactions with the concomitant reduction of V^{5+} to V^{4+} and beyond, as demonstrated for Li^+ and Na^+ [26 28]. Computed voltages are about 2.3 V vs. Mg^{2+}/Mg and 3.2 V vs. Ca^{2+}/Ca for Mg^{2+} and Ca^{2+} intercalation [21], respectively, with a specific capacity of 294.7 mAh g^{-1} related to the formation of AV_2O_5 (A = Mg, Ca). The first experimental reports on the electrochemical intercalation of Mg^{2+} into V_2O_5 date back to the late '80s, with the pioneering work of Pereira Ramos [29] and Novak [30], achieving reversible Mg insertion in V_2O_5 in $Mg(ClO_4)_2$ based electrolytes, either in dimethylsulfone at 150 °C or acetonitrile at room temperature (RT). Further attempts to electro chemically intercalate Mg^{2+} in V_2O_5 have been carried out under very diverse experimental conditions (regarding active material mor phology, electrolyte composition, temperature, cell set up and electro chemical protocols). Despite the similarity between Li^+ and Mg^{2+} ionic radius (76 and 72 pm, respectively), Mg^{2+} intercalation is hindered by its high polarizing character, which is expected to translate in slow migration kinetics and high (de)solvation energy barriers. In contrast with the vast knowledge available about the Li^+ intercalation me chanism, little is known in the case of Mg^{2+} insertion in this host,

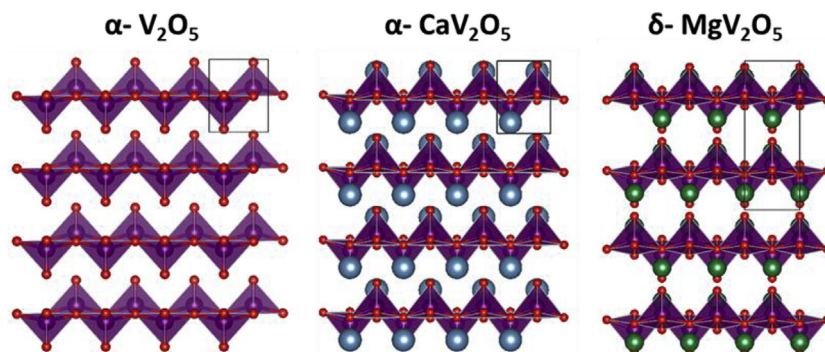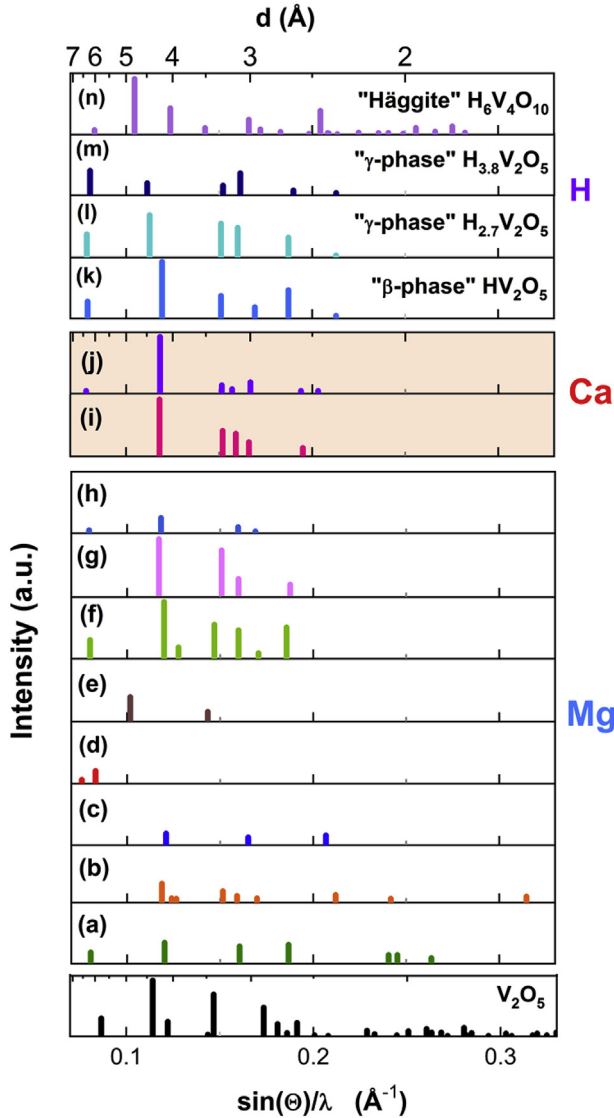**Fig. 1.** Crystal structure of the pristine α-V2O5, α-CaV$_2$O$_5$ polymorphs on the b-c plane and δ-MgV$_2$O$_5$ polymorph on the a-*b* plane.

Fig. 2. XRD peaks reported in the literature for the phases formed upon Mg^{2+} (a–h) and Ca^{2+} (i–j) electrochemical intercalation in α-V_2O_5 at RT (Ref. [17,30,33,38,39,43,48]); (k–n) Characteristic XRD reflections of chemically hydrogenated V_2O_5 phases (Ref. [44–47]). The pattern below corresponds to α-V_2O_5.

despite a significant number of publications devoted to the topic. The elucidation of the nature and crystal structure of the phase formed is still elusive and the case of Ca^{2+} is even less explored. An overview of the available literature data is provided below with a focus on the crystal chemistry and available diffraction data.

While interpretation of results converge to the existence of topo tactic insertion of very low amounts of Mg^{2+} in α V_2O_5 without major structural modifications (diffraction peaks being only slightly shifted (or broadened)) [31 38], progressive amorphization with intercalation has also been reported in some cases [17,33]. In contrast, a slight in crease of the a cell parameter has been reported after a redox process assumed to result in a significant amount of calcium intercalation in Ca inserted α V_2O_5, but no structural model is given for the phase formed [39].

Fig. 2 (panels (a j)) graphically summarizes the diffraction data available in the literature for presumably intercalated phases, formed upon electrochemical reduction of α V_2O_5. The peak intensities are re scaled between 0 and 1 (a.u.). The experimental conditions employed in each study are specified in Table 1. The actual interpretation and

assignment of the observed diffraction patterns, which can be sig nificantly different from one study to another, remains elusive in most of the cases. The Mg content within the inserted phases reported in literature has been tentatively assessed by Inductively Coupled Plasma (ICP), Atomic absorption (AAS) and Energy Dispersive (EDAX) spec troscopy or simply deduced from capacity, thus not being completely reliable. Both types of methods may yield to an overestimation of the intercalated magnesium amount: in the case of chemical methods, due to the possible existence of magnesium containing surface layers re silient to washing of the particles [40] and, in the case of electro chemical methods, due to side reactions involving cell components other than the electrode active material (mostly the electrolyte). The formation of δ MgV_2O_5 and α CaV_2O_5 isostructural to the phases pre pared by solid state reaction is generally not observed, or attribution is based on a single low intensity peak [17]. On the other hand, formation of the metastable ε $Mg_{0.5}V_2O_5$ phase has only been detected locally by aberration corrected STEM imaging [41], despite a much lower inter calation level being experimentally probed by combined atomic re solution STEM, EELS, electron diffraction and EDX techniques.

Novak and De Silvestro [42] and later other authors [17,36,43], speculated that the addition of water to the electrolyte results in en hanced electrochemical response of V_2O_5 towards magnesium inter calation basing on the higher current observed in cyclic voltammetry experiments and the higher capacity recorded. This hypothesis is re lated to the ability of H_2O molecules to strongly coordinate to magne sium ions and hence shield their high polarizing character, thus al lowing faster diffusion kinetics within the host material [16]. However, the possibility of proton (co)intercalation has never been fully dis missed and recent solid state NMR studies on electrochemically reduced (magnesiated) orthorhombic α V_2O_5 electrodes demonstrated that proton is indeed intercalated in a wet electrolyte (1 M Mg(TFSI)$_2$ in diglyme, with 2600 ppm of H_2O) [17]. These results evidence the need to consider the possible formation of hydrogenated $H_xV_2O_5$ and/or co inserted $Mg_xH_yV_2O_5$ phases for the interpretation of the XRD patterns of electrochemically reduced V_2O_5. Indeed, structural studies on the chemical hydrogenation of V_2O_5 [44] revealed that proton is initially topotactically inserted in V_2O_5 to form α $H_xV_2O_5$ (x < 0.4) phase with cell parameters only slightly different from the ones of pristine V_2O_5. At higher H^+ concentrations (*i.e.* 0.4 < x < 3.2 and 3.2 < x < 3.9), two novel orthorhombic phases are progressively formed (β and γ, re spectively), with a quasi amorphous compound (γ) obtained for x (H^+) > 3.8 [44]. The characteristic reflections of the hydrogenated β and γ $H_xV_2O_5$ phases are displayed in Fig. 2 (Panels k and l m, re spectively). This figure also exhibits the diffraction pattern of a monoclinic, "Häggite" phase with composition $H_6V_4O_{10}$ (Fig. 2 Panel n), a protonated oxide reported in 1958 by Evans and Mrose [45,46] and further observed by Srivastava et al. [47] upon chemical hydro genation of Pt activated V_2O_5 at 150 °C.

The similarities between the diffraction patterns observed after at tempts of electrochemical Mg and Ca intercalation and those of the different phases formed by chemical hydrogenation of V_2O_5 raise a question on the actual contribution of protons to the overall inter calation process, which can only be carefully assessed through addi tional characterization techniques. Despite promising steps in this di rection [17,18], detailed structural characterization of the phases formed is only starting. Interesting results have been reported by Hong et al. [43] in the course of the present work, reporting the formation of a $Mg_{0.17}H_xV_2O_5$ (0.66 < x < 1.16) phase upon reduction of sub micrometric α V_2O_5 sample in beaker type (flooded) cell at room temperature, using 0.5 M Mg(ClO$_4$)$_2$ + 2 M H_2O in ACN (acetonitrile) electrolyte (Panel g of Fig. 2). The structural model of the inserted phase is resolved through ab initio methods, by combined synchrotron XRD data and DFT calculations. The formation of another phase is observed upon further reduction, which resulted to be difficult to characterize (especially considering that the intensity of the peaks at tributed to this phase increases upon reoxidation to about 0.2 V vs Ag$^+$/

Table 1

Experimental conditions of the electrochemical intercalation tests recalled in Fig. 2 and assignments made to explain the additional diffraction peaks. ACN: Acetonitrile, G2: Diglyme, PC: Propylene Carbonate. Commercial V_2O_5 exhibits micrometric particle size.*:Phase observed after full reduction ($1.8 \leq \Delta x \leq 2$ mol e^-) and following oxidation ($2 \leq \Delta x \leq 1$ mol e^-);#: phase observed for $0.5 \leq \Delta x \leq 2$ mol e^-; ^: after reduction (2.5 cycles) and ¤: after reduction (20.5 cycles).

	W.E.	Electrolyte	C.E	Assigned Phase	Ref.
j	Commercial V_2O_5	0.5 M Ca(ClO$_4$)$_2$, ACN	CaCo$_2$O$_4$	Ca$_x$V$_2$O$_5$	[48]
i	Commercial V_2O_5	1 M Ca(ClO$_4$)$_2$, ACN	Ca	Ca$_{0.2}$V$_2$O$_5$	[39]
h	Commercial V_2O_5	0.5 M Mg(TFSI)$_2$, PC	Coated Mg	Unknown	[38]
g	Submicrometric V_2O_5	0.5 M Mg(ClO$_4$)$_2$, ACN + 2 M H$_2$O	Activated C	Unknown*	[43]
f	Submicrometric V_2O_5	0.5 M Mg(ClO$_4$)$_2$, ACN + 2 M H$_2$O	Activated C	Mg$_{0.17}$ H$_x$V$_2$O$_5$# (0.66 < x < 1.16)	[43]
e	Commercial V_2O_5	1.0 M Mg(TFSI)$_2$/G2 (15 ppm H$_2$O)	Mg	MgV$_2$O$_5$	[17]
d	Commercial V_2O_5	1.0 M Mg(TFSI)$_2$/G2 (15 ppm H$_2$O)	Mg	Unknown	[17]
c	V_2O_5 thin film	0.1 M Mg(TFSI)$_2$, ACN (32 ppm H$_2$O)	Activated C	Unknown	[33]
b	Commercial V_2O_5	1 M Mg(ClO$_4$)$_2$, ACN + 1 M H$_2$O	Mg	Mg$_x$V$_2$O$_5$ ^	[30]
a	Commercial V_2O_5	1 M Mg(ClO$_4$)$_2$, ACN + 1 M H$_2$O	Mg	Mg$_x$V$_2$O$_5$¤	[30]

Ag). However, pristine, orthorhombic α V_2O_5 was recovered upon subsequent oxidation. Surprisingly, authors state that the formation of $Mg_{0.17}H_xV_2O_5$ (together with an additional unknown phase) does also take place when the reduction is carried out in dry (2 ppm H_2O), 0.5 M Mg(ClO$_4$)$_2$ ACN electrolyte, without the formation of any other phase upon further reduction. At this point the need for a careful evaluation of the actual water content in the electrolytes is worth recalling, since conventional drying methods may not be adequate for some of the compositions used [43,49]. Moreover, alternative side reactions involving other proton sources (e.g. electrolyte breakdown reactions) should also be considered.

3. Experimental

3.1. Materials and synthesis

Commercial V_2O_5 (Sigma Aldrich, 99.6%), with micrometric particle size, was used as active material. MgV_2O_5 was synthesized either by i) solid state reaction between MgO and VO_2 [23] or by ii) comproportionation of MgV_2O_4 and MgV_2O_6. The conditions for these reactions are detailed in the following paragraphs:

i) A stoichiometric powder mixture of pre heated (500 °C, 2 h) MgO and VO_2 was annealed for 6 h at 900 °C. VO_2 was prepared by comproportionation of V_2O_5 and V_2O_3. Stoichiometric amounts of V_2O_3 and V_2O_5 powders were mixed and ground together and further annealed at 650 °C for 10 h under vacuum. Platinum sheets rolled in an Al_2O_3 crucible were employed as sample holders. The V_2O_3 precursor was prepared by reduction of V_2O_5 under pure H_2 gas flow (100 ml/min) generated by water electrolysis. Two consecutive 2 h annealing steps at 500 and 700 °C were applied and the sample was further naturally cooled under H_2 gas flow for about 10 h.

ii) Stoichiometric amounts of MgV_2O_6 and MgV_2O_4 were ground together and annealed at 770 °C for 12 h under vacuum. The MgV_2O_6 precursor was prepared by mixing V_2O_5 with a Mg^{2+} source such as MgO, Mg(OH)$_2$, or 4MgCO$_3$ ·Mg(OH)$_2$ · 5H$_2$O (independently from the Mg source employed, the same product was formed). The mixture of precursors, placed in Pt sheets rolled in Al_2O_3 crucible, was calcinated for 15 h at 650 °C in air. MgV_2O_4 was prepared by reduction of MgV_2O_6 under H_2 gas at 700 °C for 4 h.

Preparation of $Mg_xV_2O_5$ solid solutions (x = 0.7 and 0.9) was attempted by solid state reaction of MgV_2O_5 and V_2O_5 powders (mixed in x: (1 x) molar ratio) or, else, by reacting MgO, VO_2 and V_2O_5 in x: 2x: (1 x) molar ratio. In both cases, the mixed precursors were annealed at 900 °C for 6 h, under vacuum. All these resulted in mixtures of mostly MgV_2O_5 and VO_2 and thus, will not be discussed further. Alternative efforts to achieve $Mg_xV_2O_5$ (x ≤ 1) by chemical reduction of V_2O_5 with MgI$_2$ (with V_2O_5: MgI$_2$ molar ratios of 1:0.5 and 1:1 employed) also

failed. CaV$_2$O$_5$ was prepared by a comproportionation reaction from CaV$_2$O$_4$ and CaV$_2$O$_6$. Repeated annealing treatments of the mixed powder precursors were performed under vacuum at 650 °C (two 10 h steps), 750 °C (12 h) and 800 °C (two 12 h steps). Pt sheets rolled in Al_2O_3 crucibles were used as sample holders, except for the last annealing step, in which Mo crucible was employed. CaV$_2$O$_6$ was prepared by solid state reaction between CaCO$_3$ and V_2O_5 (650 °C, 12 h, air atmosphere) while CaV$_2$O$_4$ was obtained by reduction of CaV$_2$O$_6$ under H_2 gas at 700 °C for 4 h. Attempts to chemically oxidize MgV_2O_5 and CaV$_2$O$_5$ powders were made by reaction with NO$_2$BF$_4$ (100% mol excess) at 80 °C in ACN for 6 and 24 h under uninterrupted Ar bubbling. Once the reactions were completed, the samples were washed with dry ACN, vacuum filtered, dried and collected for XRD.

3.2. Structural, morphological and compositional characterization

X Ray powder diffraction patterns were acquired in a Bruker D8 Advance A25 diffractometer in a Debye Scherrer configuration equipped with Mo Kα1 radiation source (λ = 0.7093 Å) and Johansson monochromator.

High resolution synchrotron X ray diffraction (SXRD) patterns were collected at MSPD beamline (ALBA synchrotron Light Source, Cerdanyola del Vallès, Spain) using Mython detector and λ = 0.6199 Å. 0.5 mm diameter borosilicate glass capillaries were used as sample holders and rotated during data collection.

Scanning Electron Microscopy (SEM) analyses were performed with a FEI Quanta 200 FEG microscope.

Selected area electron diffraction (SAED) studies were performed using a JEOL 1210 transmission electron microscope operating at 120 kV and equipped with a Gathan sample holder. The specimens for electron microscopy were prepared dispersing the powders in dimethyl carbonate and depositing a droplet of this suspension on a carbon coated film supported on a copper grid.

3.3. Electrochemical tests

Slurries were prepared by dispersing powder mixtures of active material (80% wt), Super P carbon (10% wt) and polyvinylidene difluoride (PVdF, Kynar) binder (10% wt) in N Methyl Pyrrolidinone solvent (NMP, Sigma Aldrich). The dispersion was ball milled for 1 h at 500 Hz with a RETSCH PM100 miller before being doctor blade casted on Al foil (Goodfellow, 99%). Once casted, the tapes were dried at 120 °C under vacuum and cut into discs of 11 mm diameter, with average active material load of about 2 mg. These electrodes were pressed at 8 Tons before being used.

The electrochemical tests were performed in three electrode Swagelok cells assembled in Ar filled dry box, employing Al and stainless steel current collectors for the working and reference(RE)/counter(CE) electrodes, respectively, and Whatman borosilicate glass fiber separator soaked in 0.6 ml of electrolyte solution. Mg and Ca metal

discs were used as both counter and reference electrodes.

Dry (< 25 ppm H_2O) and wet (> 15000 ppm H_2O) solutions of 0.3 M Magnesium bis trifluoromethane sulphonyl imide ($Mg(TFSI)_2$, Solvionic, 99,5%) salt in 1:1 v mixture of ethylene carbonate (EC) and propylene carbonate (PC) (Solvionic, 99.9%) and 0.3 M Magnesium perchlorate ($Mg(ClO_4)_2$, Alfa Aesar) in EC:PC (1:1 v) were used as electrolytes for the electrochemical tests in Mg cells. In addition to those, wet (> 15000 ppm H_2O) 0.3 M $Mg(ClO_4)_2$ in ACN was also used for comparative purposes. The electrolyte solutions used in Ca experi ments were 0.45 M $Ca(BF_4)_2$, 0.3 M $Ca(ClO_4)_2$ and $Ca(TFSI)_2$ in EC:PC (1:1 v) and 0.3 M $Ca(ClO_4)_2$ in ACN with H_2O content < 25 ppm in all cases. For the sake of comparison, tests were also made with the same electrolytes exhibiting > 5000 ppm of water. The water contents of the electrolytes were measured by Karl Fisher titration.

As Mg plating cannot be achieved in $Mg(TFSI)_2$, EC:PC electrolyte at 100 °C, the electrochemical oxidation of the MgV_2O_5 phase was carried out in Li cells with Li metal as counter and reference electrodes at RT with 1 M $LiPF_6$ in EC:DMC (1:1 v) (LP30, Solvionic) or at 100 °C using an electrolyte compatible with high temperature studies: 0.1 M Lithium Bis Oxalate Borate (LiBOB, Sigma Aldrich) in EC:PC (1:1 v).

The electrochemical tests were performed on Bio Logic VMP3 and MPG2 potentiostat/galvanostats, with either potentiodynamic cycling with galvanostatic acceleration (PCGA) technique, applying potential steps of 5 mV and current threshold of C/100 (equivalent to intercala tion of one mol of divalent ions in 100 h) in order to ensure full re activity at each step, or by Galvanostatic Cycling with Potential Limitation (GCPL) at C/100 rate. Cells were left for 5 h at the open circuit potential (OCP) prior to measurements to enable temperature equilibration.

Once tested, the cells were disassembled in Ar filled dry box and the electrodes were washed with Dimethyl Carbonate solvent (DMC, Sigma Aldrich, ≥ 99%) and further collected in borosilicate glass capillaries for ex situ XRD measurements, as mentioned above.

4. Results
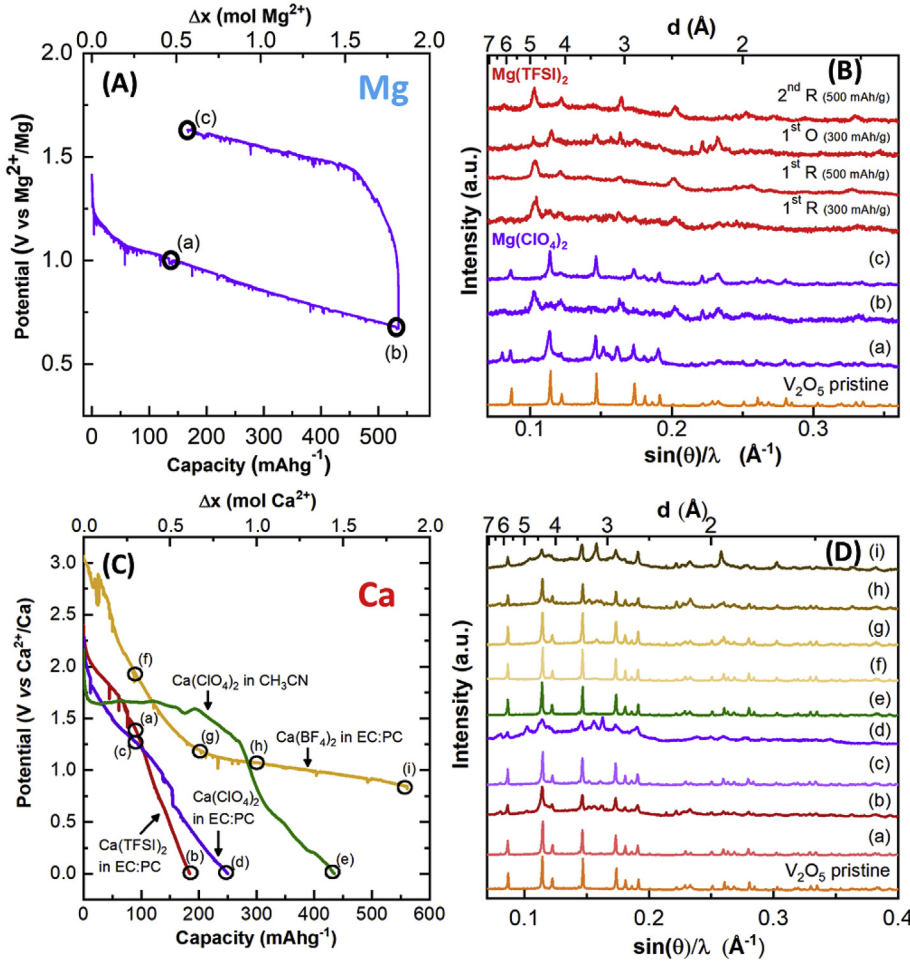
4.1. Electrochemical tests

Aiming to clarify the viability of αV_2O_5 as a reference cathode material for divalent ion battery technologies, galvanostatic cycling (GCPL) measurements were performed on V_2O_5 electrodes in Mg and Ca cells using dry alkyl carbonate based electrolyte solutions. As no elec trochemical activity was observed neither at RT nor at 55 °C, moderate temperatures of 100 °C were employed to enhance the diffusion kinetics of Mg^{2+} and Ca^{2+} (note that the efficiency of calcium plating/stripping in $CaBF_4$ in EC:PC was found to be higher at this temperature than at 50 °C) [5].

The characteristic potential vs. composition profile of V_2O_5 elec trodes subjected to GCPL tests at 100 °C and C/100 rate in Mg cells employing both 0.3 M $Mg(ClO_4)_2$ and $Mg(TFSI)_2$ in EC:PC electrolytes is displayed in Fig. 3(A). The ex situ XRD diffraction patterns of the electrodes recovered at different stages of reduction and re oxidation are displayed in Fig. 3(B). Analogous experiments were carried out in Ca cells using 0.3 M $Ca(TFSI)_2$, 0.3 M $Ca(ClO_4)_2$ and 0.45 M $Ca(BF_4)_2$ in EC:PC (1:1 v) and 1 M $Ca(ClO_4)_2$ in ACN as electrolytes (Fig. 3(C)) and the corresponding ex situ XRD patterns are presented in Fig. 3(D).

In Mg cells, the characteristic potential vs. capacity profile for V_2O_5 evolves through a continuous sloping trend upon reduction and oxi dation (Fig. 3(A)). The capacity observed is much higher than the theoretical value for full reduction of V^{+5} to V^{+4} (i.e. 294.7 mAh g^{-1}), which may reasonably be related to electrolyte decomposition side re actions, expected to be enhanced in the testing conditions employed (high temperature and very low rate). The corresponding ex situ XRD patterns at different redox stages displayed in Fig. 3(B) clearly reveal the appearance of extra peaks upon magnesiation which disappear upon oxidation up to the recovery of pristine V_2O_5. The capacity upon

reoxidation is slightly higher than theoretical, which may indicate some thermally enhanced electrolyte oxidation even at this moderate po tential. At early reduction stages in $Mg(ClO_4)_2$, EC:PC electrolyte (ca pacity close to 140 mAh g^{-1}), extra peaks were observed at d values of 3.1, 3.3, 4.2 and 6.2 Å, despite V_2O_5 being still the major phase. These peak positions are consistent with some of the patterns reported in the literature for presumably Mg^{2+} or Ca^{2+} intercalated V_2O_5, which seem also closely related to protonated $H_xV_2O_5$ phases prepared chemically (Fig. 2, panels f j and panels l m, respectively). This set of reflections was tentatively indexed with an orthorhombic Pmmn symmetry (see Fig. 4(A)) and refined using the structural model reported by Yoshi kawa et al. [44] The cell parameters obtained were a = 12.393(3), b = 3.4070(1) and c = 4.2675(1) Å (Table 2). Despite the impossibility to refine the hydrogen occupation from XRD data and the low signal to noise ratio of the pattern corresponding to the reduced sample, re finements considering a possible partial occupation of magnesium in the proton positions led to larger χ^2 values likely indicating absence of Mg^{2+} in the phase. Upon further reduction (total capacity close to 500 mAh g^{-1}), additional extra peaks formed at d = 2.45, 3.07, 4.11, 4.84 Å, while the reflections previously observed at 3.1, 3.3, 4.2 and 6.2 Å and those corresponding to V_2O_5 exhibit very low intensity if any. These peaks are consistent with the formation of a protonated Häggite type phase ($H_xV_4O_{10}$), with C2/m symmetry (see its crystal structure in Fig. S2 in S.I.). The cell parameters obtained from Rietveld refinement (Fig. 4(B)) are a = 12.437(5) Å, b = 3.043(1) Å, c = 4.926(3) Å and β = 98.48(3) Å. Note that refinement attempts placing Mg^{2+} in the proton position led to negative occupation values. Nonetheless, given the low crystallinity of the sample, the possible presence of Mg^{2+} in very low amount could not be conclusively dismissed. Similar results were obtained in $Mg(TFSI)_2$, EC:PC electrolyte, for which the ex situ XRD patterns at different redox stages are shown in Fig. 3(B) (red patterns). In this case, the Häggite type phase is the only product ob served upon full reduction (500 mAh/g). Similar XRD patterns were also obtained after GCPL tests on cells with magnesiated active carbon as counter electrode and for both $Mg(ClO_4)_2$ and $Mg(TFSI)_2$ based electrolytes, allowing to detect the formation of the Häggite type phase again after a second reduction.

The potential vs. capacity profile for experiments carried out in Ca cells at C/100 rate, depicted in Fig. 3(C), revealed to be significantly dependent on the electrolyte used: for $Ca(TFSI)_2$ and $Ca(ClO_4)_2$ in EC:PC 1:1v the profile follows a sloping trend down to specific capacity values between 180 and 250 mAhg^{-1} while for $Ca(ClO_4)_2$ in ACN at RT, a plateau at 1.7 V vs. Ca^{2+}/Ca is observed up to specific capacities of 300 mAh g^{-1} followed by a sloping region up to 430 mAh g^{-1} at 0 V vs. Ca^{2+}/Ca in agreement with previous reports [39]. In the case of Ca $(BF_4)_2$ in EC:PC a plateau is reached at 1.2 V vs. Ca^{2+}/Ca which extends to a specific capacity of 550 mAh g^{-1}. It is worth mentioning that the OCP observed in $Ca(BF_4)_2$ electrolyte is approximatively 0.7 V higher than those observed for the other three electrolytes, which might be related to the formation of different passivation layers on the Ca RE. The ex situ XRD patterns of the V_2O_5 electrodes taken at different re duction stages are displayed in Fig. 3(D). No additional reflections are observed at early stages of reduction (> 1.2 V vs. Ca^{2+}/Ca, < 100 mAh g^{-1}) in any of the electrolytes tested and only a very minor change in lattice parameters of V_2O_5, if any, is detected (see Fig. S1 in S.I.), which points at ascribing the observed capacity to side reactions most likely involving the electrolyte. Upon further reduction additional peaks are observed at 3.1, 3.3, 4.2 and 6.2 Å (see Fig. 3(D) patterns (b), (d), (h) and (i)]. These reflections, appearing at the same d values as those observed for Mg cells (see Fig. 3(B)), seem compatible with the patterns of electrochemically reduced and chemically protonated V_2O_5 phases reported in literature (Fig. 2, panels f j and 2, panels l m, respectively). Only in the case of $Ca(ClO_4)_2$ in EC:PC 1:1 v the appearance of other peaks, the most intense at d = 4.85 Å is observed upon full reduction (see Fig. 3(D) pattern (d)), which seems to correspond to the Häggite phase ($H_xV_4O_{10}$) observed in the Mg experiments previously discussed

Fig. 3. (A) Characteristic GCPL voltage profile versus specific capacity (bottom axis) and versus moles of inserted ion (Δx) (top axis), considering that all electrochemical response is related to divalent ion intercalation, of a Mg/0.3 M Mg(ClO₄)₂, EC:PC (1:1 v)/V₂O₅ cell (C/100 rate, 100 °C) and corresponding ex-situ XRD patterns **(B).** The XRD patterns of V₂O₅ upon cycling in Mg(TFSI)₂ electrolyte (C/100 rate, 100 °C) are also shown in **(B)**; **(C)** Characteristic GCPL voltage profile (C/100 rate) versus specific capacity (bottom axes) and versus hypothetical number of moles of inserted ion (Δx) (top axes) of Ca/0.3 M Ca(TFSI)₂, EC:PC (1:1 v)/V₂O₅ cell, 100 °C (red line), Ca/0.3 M Ca(ClO₄)₂, EC:PC (1:1 v)/V₂O₅ cell, 100 °C (purple line), Ca/1 M Ca(ClO₄)₂ EC:PC (1:1 v)/V₂O₅ cell, 100 °C, Ca/0.3 M Ca(ClO₄)₂, ACN/V₂O₅ cell, RT (green line), Ca/0.45 M Ca(BF₄)₂, EC:PC (1:1 v)/V₂O₅ cell, 100 °C (yellow line) and corresponding ex-situ XRD patterns **(D)** The pattern of pristine V₂O₅ is also given for comparison. (For interpretation of the references to color in this figure legend, the reader is referred to the Web version of this article.)

(see Fig. 3(B)). After significant reduction in Ca(BF₄)₂ electrolyte (Fig. 3(D) pattern (i)) two peaks at d values of 1.93 and 3.16 Å are indicative of the formation of CaF₂. Thus, we speculate that the long plateau observed in the GCPL curve is related to the electrolyte de composition. Finally, despite the capacity observed upon reduction at RT using Ca(ClO₄)₂ in ACN as electrolyte, no changes in the XRD pattern can be detected (see Fig. 3(E) pattern (e)) and hence we are tempted to again ascribe it to side reactions involving the electrolyte.

The effect of water impurities in the electrolyte on the electro chemical response of the V₂O₅ electrodes in Mg and Ca cells was in vestigated by performing galvanostatic cycling at C/100 rate and both RT and 100 °C in wet electrolytes (water content between 4000 ppm and 18000 ppm) (Fig. S3) and carrying out ex situ XRD experiments (Fig. 5(A) and (B)). Independently from the temperature, enhanced specific capacities are recorded in the water containing electrolytes as compared to the dry ones (See Fig. S3 (A) and (B) in the S.I.). For in stance, in Mg cells (Mg(ClO₄)₂,EC:PC; 100 °C) about 500 mAh g⁻¹ were recorded when V₂O₅ was reduced down to 0.7 V vs Mg²⁺/Mg in dry electrolyte (Fig. 3A), while cycling in wet electrolyte led to a capacity of almost 600 mAh g⁻¹ with a cutoff voltage above 1 V vs Mg²⁺/Mg (Fig. S3A) reasonably including contributions from uncontrolled side reac tions (possibly including water reduction).

The lattice parameters of V₂O₅ remained virtually unchanged after the reduction tests performed in both Ca and Mg cells. The appearance of additional reflections at d values of 3.2, 4.15 and 6.4 Å was observed upon both presumed magnesiation and calciation, independently from the electrolyte and temperature. These values are close to those ob served after galvanostatic reduction tests in dry Mg and Ca electrolytes previously discussed and may be tentatively assigned to an

orthorhombic phase related to γ HₓV₂O₅. It is important to highlight that this orthorhombic V₂O₅ related secondary phase, characterized by a larger a cell parameter, appears in a meaningful fraction at room temperature in presence of water (Fig. 5(A) patterns (a), (b) and (d)) and its formation seems to be favored by both water and temperature.

Furthermore, the main peak of the Häggite phase (HₓV₄O₁₀) at d value of 4.8 Å was also observed in the samples reduced in Mg(ClO₄)₂, EC:PC + H₂O at 100 °C and in wet Ca(TFSI)₂ and Ca (ClO₄)₂EC:PC + H₂O electrolytes at RT (Fig. 5(A) pattern (c) and Fig. 5(B) patterns (b) and (c), respectively). In the case of wet Ca(BF₄)₂ electrolyte, peaks corresponding to V₂O₅ were no longer observable and the pattern presented only the peaks at d = 3.2, 4.15 and 6.4 Å. The position and intensities of these peaks seen again compatible with a phase related to γ HₓV₂O₅ with an a parameter further expanded to approximatively 12.86 Å inducing the reflections (110) and (400) to merge (see Fig. S9 in S.I.).

4.2. Evolution of electrodes at OCP

Aiming to detect any possible evolution of the α V₂O₅ electrodes resulting from contact with the electrolyte that could bias the results of the electrochemical tests, different cells were assembled and kept at OCP (i.e. without any current applied) at different temperatures for various periods of time. The cells were then opened and the electrodes recovered and characterized. Fig. 6(A) and (B) display the corre sponding ex situ XRD patterns of V₂O₅ electrodes, in Mg and Ca cells respectively.

As noticeable in Fig. 6(A) (pattern (c), extra peaks at d values of 6.2, 4.9, 3.3 and 3.1 Å, were observed after 100 h at OCP at 100 °C in
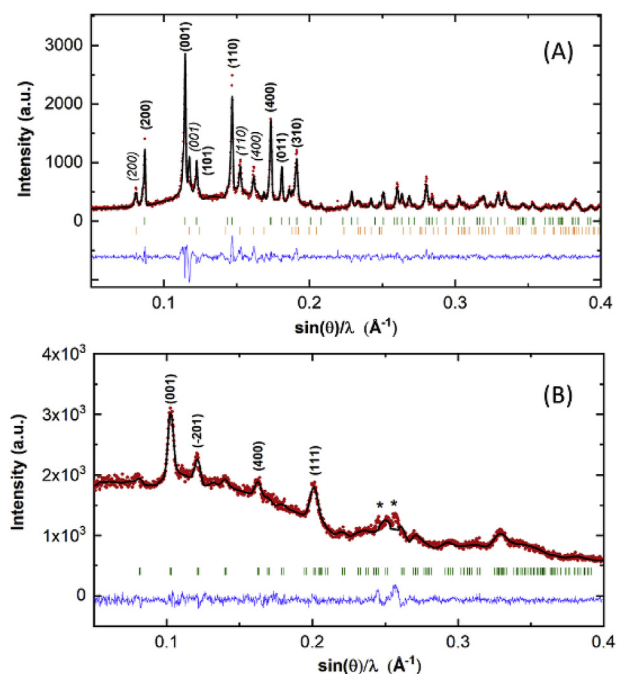
Fig. 4. Observed and calculated X-ray powder diffraction patterns of V_2O_5 tape electrode **(A)** partially reduced (140 mAh g^{-1}) in 0.3 M Mg(ClO$_4$)$_2$ EC:PC (1:1 v), **(B)** at full reduction (500 mAhg^{-1}) in 0.3 M Mg(TFSI)$_2$ EC:PC (1:1v). Tick marks indicate allowed reflections for α-V$_2$O$_5$ (Upper set in **(A)**), H$_x$V$_2$O$_5$ (lower set in **(A)**) and Häggite phase H$_6$V$_4$O$_{10}$ (green ticks in **(B)**). Reflections indicated with * are instrumental contribution due to direct beam stoppers. (For interpretation of the references to color in this figure legend, the reader is referred to the Web version of this article.)

Table 2
Crystallographic data refined for V$_2$O$_5$ electrode after partial reduction (140 mAh g^{-1}) in 0.3 M Mg(ClO$_4$)$_2$ EC:PC (1:1 v) and full reduction (500 mAh g^{-1}) in 0.3 M Mg(TFSI)$_2$ EC:PC (1:1 v).

|	α-V$_2$O$_5$	γ-H$_x$V$_2$O$_5$	H$_6$V$_4$O$_{10}$
Radiation	X-ray Mo k$_{\alpha1}$	X-ray Mo k$_{\alpha1}$	X-ray Mo k$_{\alpha1}$
System	Orthorhombic	Orthorhombic	Monoclinic
Space group	Pmmn	Pmmn	C2/m
a (Å)	11.540(2)	12.393(3)	12.437(5)
b (Å)	3.5697(4)	3.4070(1)	3.043(1)
c (Å)	4.3703(6)	4.2675(1)	4.926(3)
β (°)	90.0	90.0	98.48(3)

0.3 M Mg(TFSI)$_2$, EC:PC 1:1 v electrolyte. Such peaks were not observed when the tests were carried out at RT (a) and at 100 °C for shorter time (i.e. 24 h, pattern (b)). Furthermore, a progressive phase amorphization could be detected at 100 °C. In contrast, no evolution of the diffraction pattern was detected in 0.3 M Mg(ClO$_4$)$_2$, EC:PC 1:1 v electrolyte even after OCP for 100 h at 100 °C (d), which indicates possible effects of the electrolyte salt anion on the reactivity towards the electrolyte. The ex situ XRD patterns after 4 days OCP in Ca cells at RT in dry 0.3 M Ca(TFSI)$_2$, 0.3 M Ca(ClO$_4$)$_2$, 0.45 M Ca(BF$_4$)$_2$ in EC:PC 1:1 v or 0.3 M Ca(ClO$_4$)$_2$ in ACN electrolytes did not present any observable sign of degradation (Fig. S4 S.I.). Moreover, no degradation was noticed even after 7 days in 0.3 M Ca(TFSI)$_2$ and 0.3 M Ca(ClO$_4$)$_2$ at 100 °C in EC:PC 1:1 v as shown in Fig. 6(B) (pattern (a) and (b)). The peaks at d values of 6.2, 4.9, 3.3 Å could be observed when 0.45 M Ca(BF$_4$)$_2$ in EC:PC was used, which points also to an effect of the electrolyte salt anion on the overall active phase/electrolyte side reactivity. Interestingly, the positions of these reflections are similar to those observed in early stages of reduction in several Mg^{2+} and Ca^{2+} dry electrolytes (see Fig. 3(B) and (D) (pattern (b) and (d), (h), respectively) and, in a greater fraction, in all electrodes reduced in wet electrolytes, independently of the electrolyte and temperature. As discussed earlier, these peaks are consistent with the patterns reported in the literature for presumably Mg^{2+} or Ca^{2+} intercalated V$_2$O$_5$ which seem closely related with those of chemically obtained H$_x$V$_2$O$_5$ phases (Fig. 2, panels f j and panels l m, respectively). Such findings seem again to indicate that the orthorhombic V$_2$O$_5$ related phase, characterized by a larger a cell parameter, is most likely related to a degradation of V$_2$O$_5$ electrochemically favored in wet electrolyte at high temperature but also spontaneously formed upon prolonged exposure to dry electrolyte.

4.3. V$_2$O$_5$ stability

With the aim to rationalize the results discussed above and to understand the effect of the different electrolyte components (salt and solvent) in the reactivity observed, further experiments were carried out by simply soaking pristine V$_2$O$_5$ powder at RT and 100 °C in diverse electrolytes including bare solvents. Changes in the suspension color, indicative of possible reduction of V^{+5}, were observed to gradually grow upon time at 100 °C, even in pure alkylcarbonate solvents. The XRD patterns of such samples revealed the presence of a set of additional peaks, the most intense at d = 3.2 Å. These peaks are found to grow with time. After 6 weeks in EC:PC (1:1 v) at 100 °C the new phase with main reflections at d = 3.2, 4.15 and 6.4 Å is predominant and peaks corresponding to pristine V$_2$O$_5$ have very low intensity. (See Figs. S5 and S6 in the S.I.). These stability test has evidenced that this orthorhombic V$_2$O$_5$ related phase observed after 100 h at OCP at 100 °C in 0.3 M Mg(TFSI)$_2$ or Ca(BF$_4$)$_2$, EC:PC 1:1 v and in reduction in wet or dry
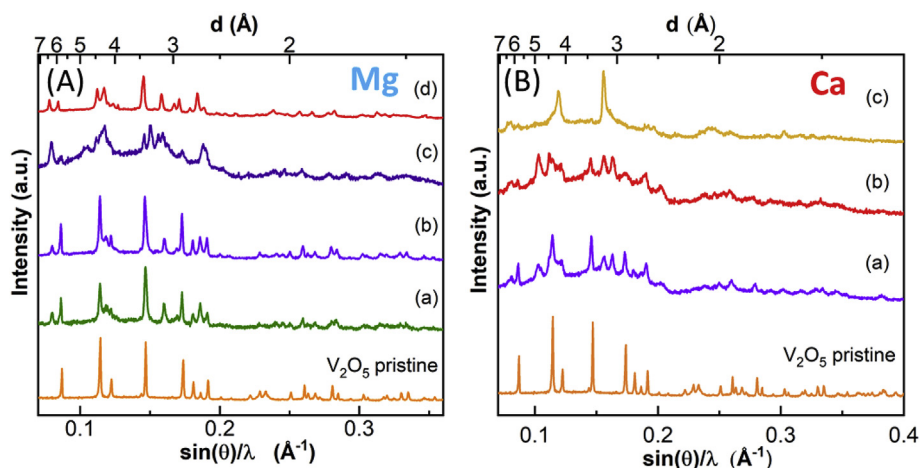
Fig. 5. (A) Ex-situ XRD patterns of the V$_2$O$_5$ electrode after galvanostatic reduction at C/100 rate in 0.5 M Mg(ClO$_4$)$_2$, ACN + 1 M H$_2$O at RT (500 mAh/g): **(a)** 0.3 M Mg(ClO$_4$)$_2$, EC:PC + 1 M H$_2$O at RT (200 mAh/g); **(b)** 100 °C (600 mAh/g); **(c)** in 0.3 M Mg(TFSI)$_2$, EC:PC + 1 M H$_2$O at RT (120 mAh/g) **(d)**. **(B)** Ex-situ XRD patterns of V$_2$O$_5$ after reduction at 100 °C and C/100 rate in **(a)** 0,3 M Ca(ClO$_4$)$_2$, EC:PC + H$_2$O (280 mAh/g) **(b)** 0,3 M Ca(TFSI)$_2$, EC:PC: H$_2$O (410 mAh/g) and **(c)** 0,45 M Ca(BF$_4$)$_2$, EC:PC + H$_2$O (390 mAh/g).
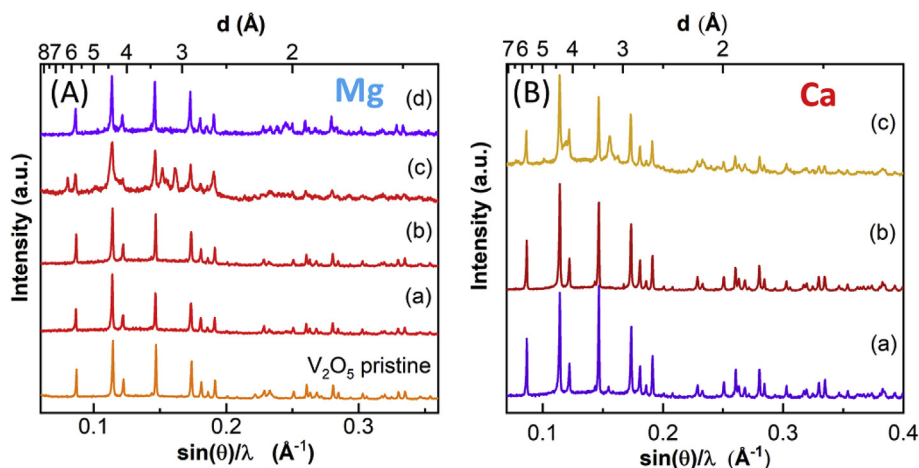
Fig. 6. Ex-situ XRD patterns of the V_2O_5 electrodes after OCP tests in Mg **(A)** and Ca **(B)** 2-electrode cells. **(A)** 0.3 M Mg(TFSI)$_2$, EC:PC 1:1 v (red plots): **(a)** 100 h at RT, **(b)** 24 h at 100 °C, **(c)** 100 h at 100 °C and 0.3 M Mg(ClO$_4$)$_2$, **(d)** EC:PC 1:1 v (violet plot) after 100 h OCP at 100 °C. The diffraction pattern of pristine V_2O_5 phase is also given for comparison. **(B)** Ex-situ XRD patterns after 1 week OCV at 100 °C in **(a)** 0.3 M Ca(ClO$_4$)$_2$/EC:PC, **(b)** 0.3 M Ca(TFSI)$_2$/EC:PC, **(c)** 0.45 M Ca(BF$_4$)$_2$/EC:PC. (For interpretation of the references to color in this figure legend, the reader is referred to the Web version of this article.)

electrolyte are also spontaneously formed after long exposition of V_2O_5 to pure dry EC:PC electrolyte at 100 °C and are thus presumably related to the same phase(s). However, no significant evolution could be detected in the XRD patterns of the powders soaked for 1 week in an electrolyte containing Mg(TFSI)$_2$ and Mg(ClO$_4$)$_2$ based electrolytes, which indicates that the degree of degradation, if any, was small or either resulted in amorphous side products.

Even if a thorough understanding of the possible mechanisms underneath the V_2O_5 reductive decompositions goes beyond the scope of the present study, additional experiments aiming at shedding some light on the transformations undergone by V_2O_5 at 100 °C in alkyl carbonate based electrolytes were conducted. Since a previous TEM study of the V_2O_5 thermal decomposition process [50] revealed that VO_x and 7 and 24 fold superstructure phases related to oxygen loss and vacancy ordering could be locally observed in V_2O_5 samples annealed at 100 °C for 5 days, we decided to carry out electron diffraction to further characterize the phase resulting from V_2O_5 reactivity with the electrolyte. Fig. 7 displays a comparison of the representative SAED patterns along the [001] and [012] zone axes of the V_2O_5 powder sample in its pristine state (**(A)** and **(C)**, respectively) and after 100 h at OCP at 100 °C (**(B)** and **(D)**, respectively). As expected, reconstruction of the reciprocal space, obtained by tilting around the a* axis for pristine V_2O_5, led to the determination of the cell parameters (a = 11.53 Å, b = 3.59 Å and c = 4.36 Å) with the observed reflections being consistent with the orthorhombic space group Pmmn (No. 59) [51]. In contrast, an additional phase was detected in the sample stored for 100 h at OCP at 100 °C. The reconstruction of the reciprocal space from SAED patterns yielded an orthorhombic cell with cell parameters a = 12.39 Å b = 3.44 Å and c = 8.25 Å, which are somewhat related to those of pristine V_2O_5 (a = 11.53 Å, b = 3.59 Å, c = 4.36 Å), with a longer a parameter and doubling of c. Furthermore, weak additional reflections are observed in several planes, such as those marked with orange arrows in the [001] pattern of Fig. 7(B), which, according to Tilley et al. [50], can be interpreted as twins due to the presence of a VO_x phase.

Besides giving further proof of the reactivity of V_2O_5 at moderate temperature (100 °C) in contact with electrolyte components, these observations open the room for speculation about reaction mechanisms. Indeed, in addition to chemical redox reaction involving proton (coming from water impurities or electrolyte side reactions) or divalent cation intercalation, oxygen loss seems to also be plausible, but in this case no reversibility could be expected.

4.4. AV_2O_5 (A = Mg, Ca): synthesis and electrochemical reactivity

Given the impossibility to achieve significant multivalent intercalation into V_2O_5, we approached the subject from the opposite side,

by synthesizing fully intercalated AV_2O_5 (A: Mg, Ca) phases and investigating the viability of MV ion extraction both electrochemically and chemically.

Pure, orthorhombic δ MgV_2O_5 phase (S.G. Cmcm) was obtained either by i) direct synthesis from MgO and VO_2 or by ii) comproportionation reaction of MgV_2O_6 and MgV_2O_4, with cell parameters of a = 3.6920(4) Å, b = 9.9737(1) Å and c = 11.0208(10) Å and a = 3.6908(2) Å, b = 9.9747(7) Å and c = 11.0229(6) Å for i) and ii), respectively. Both syntheses, described in the Experimental section, led to the formation of micrometric δ MgV_2O_5, however with slight differences in the particle morphology (See Fig. S8 in S.I.).

Orthorhombic α CaV_2O_5 phase (S.G. Pmmn) with cell parameters a = 11.3310(9) Å, b = 3.605(3) Å and c = 4.9000 (4) Å was obtained by comproportionation reaction of CaV_2O_6 and CaV_2O_4 (See the Experimental Section for details). The concomitant formation of V_2O_3 (S.G. R 3c) and $Ca_3V_2O_8$ (R3c) as impurity phases in amounts approaching, respectively, 7% and 2% in weight, could not be avoided by repeated annealing treatments (See Fig. S8 in S.I.)

Attempts to chemically deintercalate Mg^{2+} from MgV_2O_5 by reaction with NO_2BF_4 at 80 °C in ACN did not result in any change in the crystal structure (See Fig. 8(A)) and no meaningful variation of the cell parameters was inferred from Rietveld refinement. When reacted with NO_2BF_4 oxidant in ACN at 80 °C, the brown CaV_2O_5 powder samples got rapidly dissolved and formed blue colored suspensions indicating the presence of V^{+4}. The XRD pattern of the powder after decantation of the obtained suspension revealed the formation of an amorphous phase together with broadened and noisy reflections tentatively ascribed to V O phases, with triclinic V_4O_7 appearing as one of the possible compounds present. However, the breath of the peaks and low signal to noise ratio in the patterns hampered any unambiguous peak indexing. The electrochemical oxidation tests revealed that the AV_2O_5 (A: Mg, Ca) phases are inactive at RT while specific capacities approaching the theoretical value (i.e. Δx = 1 mol A^{2+}) could be achieved at 100 °C, with voltage profiles displaying a plateau between 3.8 and 4.2 V vs Li^+/ Li and between 3.4 and 3.55 V vs Ca^{2+}/Ca for the MgV_2O_5 and the CaV_2O_5 electrodes, respectively (See Fig. S9 (A) and (B) in S.I.) The ex situ XRD patterns of the oxidized samples (Fig. 8 (A) and (B)) revealed neither meaningful variation of the cell parameters nor phase amorphization with respect to the pristine phases. The extra reflections observed in the ex situ XRD diffractograms of the electrochemically oxidized MgV_2O_5 phase may be ascribed to $Li_xB_yO_z$ phases, reasonably due to electrolyte salt (LiBOB) decomposition.

5. Discussion

The results from this study evidence that V_2O_5 is electrochemically inactive towards MV ion intercalation at RT in dry electrolyte solutions.
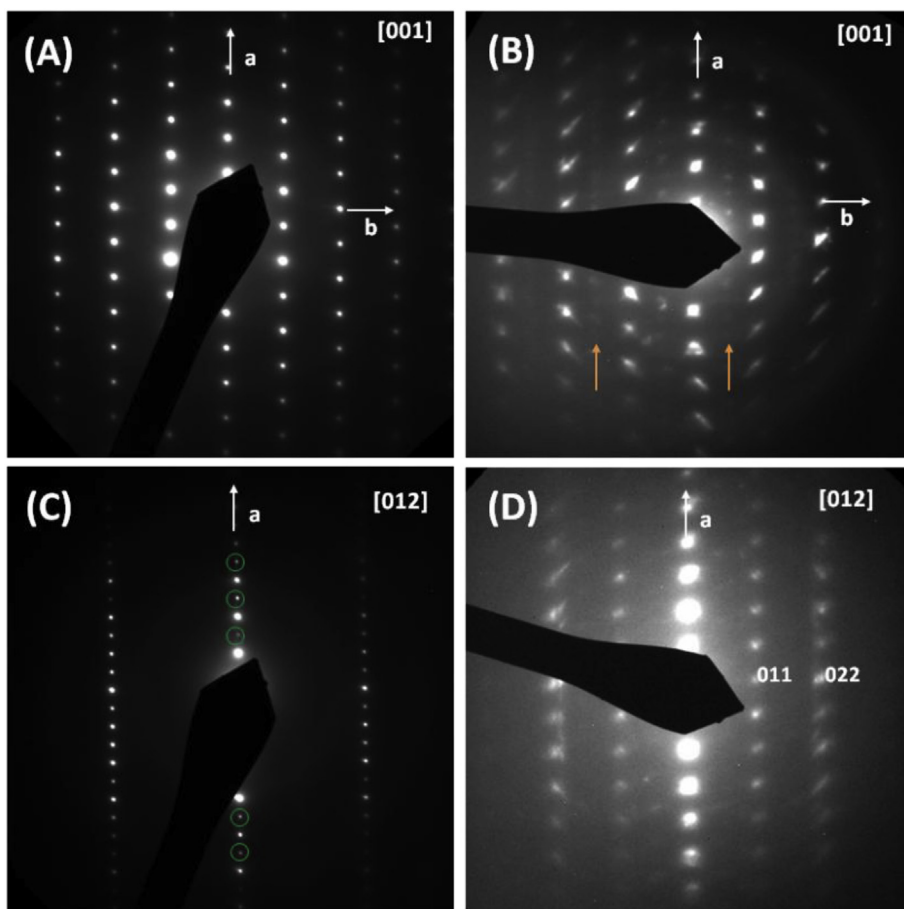
Fig. 7. Electron diffraction patterns corresponding to [100] and [012] zone axis for V_2O_5 pristine [(a), (c)] and after 100 h at the OCP at 100 °C [(b), (d)]. The green circles marked in (c) correspond to double diffraction and the orange arrows marked in (b) indicate possible twins. (For interpretation of the references to color in this figure legend, the reader is referred to the Web version of this article.)

In contrast, relatively high values of specific capacity are obtained either by increasing the testing temperature to 100 °C or by increasing the water content in the electrolyte. Despite not being able to fully elucidate all the side reactions taking place and the phases involved, our findings unambiguously show that V_2O_5 is not stable in contact with the electrolytes (or even the electrolyte solvents alone) at 100 °C and that partial reduction of V^{+5} takes place. Hence, even if it is clear that applied current may modify the degradation mechanism, thermal instability has to be considered when assessing the results of electrochemical tests done above RT. The extent of the V_2O_5 reductive decomposition reaction is enhanced with time, but also depends on the electrolyte composition, being higher for magnesium than for calcium based electrolytes, the lowest degradation being observed with

$A(ClO_4)_2$ (A = Mg, Ca) salts. Whether the charge compensation mechanism is related to oxygen loss (presumably irreversible), proton intercalation or both, is unclear at this stage and the nature of the phases formed is not unambiguously elucidated. Furthermore, the source of protons is also a matter of debate: since electrolytes with very low water contents were used in our study, we speculate that protons may alternatively come from complex decomposition reactions involving most likely electrolyte solvents, but further studies beyond the scope of the present paper should be carried out to assess that point. Yet, this is in agreement with previous work by Hong et al. [43] reporting the formation of similar phases upon electrochemical magnesiation of V_2O_5 in both dry and wet electrolytes.

Despite a significant part of the electrochemical capacity observed
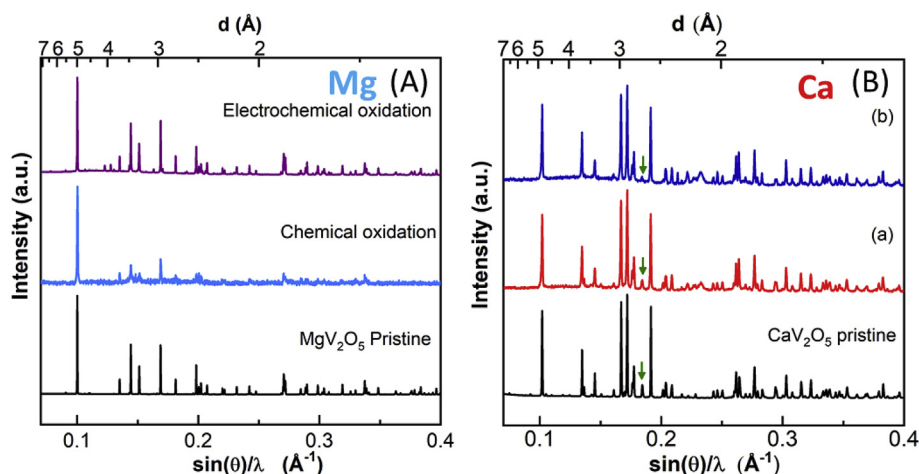
Fig. 8. Ex-situ XRD patterns of (A) MgV_2O_5 pristine electrode (black) and after chemical (light blue) and electrochemical (purple) oxidation; (B) CaV_2O_5 pristine electrode (black): (a) after 7 days OCP and (b) after electrochemical oxidation in $Ca(BF_4)_2$/ EC:PC at 100 °C. Green arrow indicates the main peak of V_2O_3 impurity. (For interpretation of the references to color in this figure legend, the reader is referred to the Web version of this article.)

in the experiments being related to side reactions involving the electrolyte (especially for $Ca(BF_4)_2$), changes in the diffraction pattern of V_2O_5 upon reduction at 100 °C are clearly observed, with variations being more evident in Mg than in Ca cells. In some of the electrolytes employed (such as the case of $Mg(ClO_4)_2$ in EC:PC), no evident signs of V_2O_5 thermal degradation could be detected by XRD (neither after OCP nor after soaking experiments), while sets of peaks due to the formation of additional phases were clearly observed along the reduction process. Besides the formation of phases analogous to those formed after long OCP periods (in amounts dependent on the employed electrolyte), the full reduction experiments led to the formation of a Häggite type phase with a negligible divalent ion content, if any. In this respect, the formation of a fully inserted MgV_2O_5 or CaV_2O_5 phase was unambiguously dismissed by Rietveld refinement, this addressing a critical point in the controversial literature background related to the topic. The formation of a Häggite type phase was observed both in Mg and Ca cells (on a minor extent in dry electrolytes than in wet ones). The reversibility of this reaction (despite some loss of crystallinity) does again raise the question of the competition between divalent and proton intercalation and points to the existence of alternative proton sources other than water impurities in the electrolyte.

Last but not least, no changes in the diffraction pattern were observed at RT unless water was added to the electrolyte. Despite the stability of V_2O_5 in the electrolyte at RT, its reduction in Mg cells with wet electrolytes led to the formation of a phase consistent with the one formed upon degradation at 100 °C (both at the OCP and upon reduction in Mg cells and in Ca cells only with $Ca(BF_4)_2$ based electrolyte). The diffraction pattern observed seems closely related to chemically prepared γ $H_xV_2O_5$ phases, which do also bear strong similarities with most of the patterns reported in the literature upon presumable MV ion intercalation in dry and wet electrolytes at RT.

The results achieved in the course of this study indicate that, despite the similarity between the AV_2O_5 (A = Ca, Mg) and V_2O_5 crystal structures, the formation of a solid solution between α V_2O_5 and α CaV_2O_5 is not possible, neither electrochemically nor chemically. Moreover, attempts to intercalate magnesium in α V_2O_5 do not lead to the formation of the closely related δ MgV_2O_5. While for the case of the α polymorphs this can be related to higher migration barriers, in agreement with DFT results, the impossibility to extract Mg^{2+} from δ MgV_2O_5 either chemically or electrochemically comes as a surprise, as moderate migration barriers were predicted in this polymorph [20]. Our most relevant and puzzling observations relate to the existence of several possible side reactions during the electrochemical reduction of α V_2O_5 related to thermal instability or reactivity with the electrolyte components and water impurities. Unfortunately, none of the experiments performed enabled to assess a true significant amount of Ca^{2+} or Mg^{2+} intercalation in α V_2O_5. While surprising at first sight, this is consistent with the controversial data available from previous literature, evidencing the impossibility to extract meaningful structural correlations from diffraction patterns with low signal to noise ratio or broad peaks.

6. Conclusions

The results obtained in this study contribute to raise the awareness about open questions related to MV ion intercalation into α V_2O_5, generally regarded as a prototypical cathode host for MV batteries even without a clear understanding of the overall intercalation process, especially from a crystal chemistry perspective.

Our findings shed some light into the existing controversy and point at the unsuitability of V_2O_5 as cathode for Mg and Ca batteries. Indeed, no evidence of significant MV ion intercalation can be inferred from the refinements of the ex situ XRD patterns of the electrodes collected after electrochemical reduction experiments carried out under various conditions. The formation of protonated Häggite type phases $H_xV_4O_6$ (C2/m symmetry) rather than magnesiated or calciated V_2O_5 is observed in

both dry and wet electrolytes, with protons most likely coming from complex electrolyte decomposition requiring further studies to be fully understood.

Furthermore, a thorough analysis of the XRD pattern of V_2O_5 stored in the employed electrolytes (or even in the bare solvents) or in Mg and Ca cells kept at the OCP revealed the progressive appearance of a set of peaks closely related to those of chemically prepared γ $H_xV_2O_5$. These patterns are also similar to most of those reported in the literature after presumable MV ion intercalation in dry and wet electrolytes at RT, its origin being not even tentatively elucidated in most of the cases. Our findings are consistent with this orthorhombic V_2O_5 like phase with expanded a parameter resulting from a reductive decomposition of V_2O_5 that requires further investigation.

The surprising results achieved in the course of this study underpin the importance of a rigorous methodology for a thorough and reliable investigation of the reduction process. Thermal and chemical stabilities need to be assessed, especially for tests done above RT, and characterization techniques complementary to electrochemistry are compulsory to demonstrate MV ion intercalation.

Appendix A. Supplementary data

Supplementary data related to this article can be found at https://doi.org/10.1016/j.jpowsour.2018.08.024.

References

[1] J. Muldoon, C.B. Bucur, T. Gregory, Quest for nonaqueous multivalent secondary batteries: magnesium and beyond, Chem. Rev. 114 (2014) 11683–11720, https://doi.org/10.1021/cr500049y.

[2] D. Aurbach, Z. Lu, A. Schechter, Y. Gofer, H. Gizbar, R. Turgeman, Y. Cohen, M. Moshkovich, E. Levi, Prototype systems for rechargeable magnesium batteries, Nature 407 (2000) 724–727, https://doi.org/10.1038/35037553.

[3] J.W. Choi, D. Aurbach, Promise and reality of post-lithium-ion batteries with high energy densities, Nat. Rev. Mater. 1 (2016) 1–16, https://doi.org/10.1038/natrevmats.2016.13.

[4] H.D. Yoo, I. Shterenberg, Y. Gofer, G. Gershinsky, N. Pour, D. Aurbach, Mg rechargeable batteries: an on-going challenge, Energy Environ. Sci. 6 (2013) 2265–2279, https://doi.org/10.1039/c3ee40871j.

[5] A. Ponrouch, C. Frontera, F. Bardé, M.R. Palacín, Towards a calcium-based rechargeable battery, Nat. Mater. 15 (2015) 1–5, https://doi.org/10.1038/nmat4462.

[6] D. Wang, X. Gao, Y. Chen, L. Jin, C. Kuss, P.G. Bruce, Plating and stripping calcium in an organic electrolyte, Nat. Mater. 17 (2018) 16–20, https://doi.org/10.1038/NMAT5036.

[7] M.E. Arroyo-de Dompablo, C. Krich, J. Nava-Avendaño, N. Biškup, M.R. Palacín, F. Bardé, A joint computational and experimental evaluation of $CaMn_2O_4$ polymorphs as cathode materials for Ca ion batteries, Chem. Mater. 28 (2016) 6886–6893, https://doi.org/10.1021/acs.chemmater.6b02146.

[8] M.E. Arroyo-de Dompablo, C. Krich, J. Nava-Avendaño, M.R. Palacín, F. Bardé, In quest of cathode materials for Ca ion batteries: the $CaMO_3$ perovskites (M = Mo, Cr, Mn, Fe, Co, and Ni), Phys. Chem. Chem. Phys. 18 (2016) 19966–19972, https://doi.org/10.1039/C6CP03381D.

[9] R. Verrelli, M.E. Arroyo-de Dompablo, D. Tchitchekova, A.P. Black, C. Frontera, A. Fuertes, M.R. Palacín, On the viability of Mg extraction in $MgMoN_2$: a combined experimental and theoretical approach, Phys. Chem. Chem. Phys. 19 (2017) 26435–26441, https://doi.org/10.1039/C7CP04850E.

[10] D. Tchitchekova, A. Ponrouch, R. Verrelli, T. Broux, C. Frontera, A. Sorrentino, F. Barde, N. Biskup, M.E. Arroyo-de Dompablo, M.R. Palacin, Electrochemical intercalation of calcium and magnesium in TiS_2: fundamental studies related to multivalent battery applications, Chem. Mater. 30 (2018) 847–856, https://doi.org/10.1021/acs.chemmater.7b04406.

[11] D.S. Tchitchekova, D. Monti, P. Johansson, F. Bardé, A. Randon-Vitanova, M.R. Palacín, A. Ponrouch, On the reliability of half-cell tests for monovalent (Li^+, Na^+) and divalent (Mg^{2+}, Ca^{2+}) cation based batteries, J. Electrochem. Soc. 164

(2017) A1384–A1392, https://doi.org/10.1149/2.0411707jes.

[12] A.L. Lipson, D.L. Proffit, B. Pan, T.T. Fister, C. Liao, A.K. Burrell, J.T. Vaughey, B.J. Ingram, Current collector corrosion in Ca-Ion batteries, J. Electrochem. Soc. 162 (2015) A1574–A1578, https://doi.org/10.1149/2.0811508jes.

[13] D.L. Proffit, T.T. Fister, S. Kim, B. Pan, C. Liao, J.T. Vaughey, Utilization of Ca K-Edge x-ray absorption near edge structure to identify intercalation in potential multivalent battery materials, J. Electrochem. Soc. 163 (2016) A2508–A2514, https://doi.org/10.1149/2.0121613jes.

[14] L. Li, Y.-C.K. Chen-Wiegart, J.J. Wang, P. Gao, Q. Ding, Y.-S. Yu, F. Wang, J. Cabana, J.J. Wang, S. Jin, Visualization of electrochemically driven solid-state phase transformations using operando hard X-ray spectro-imaging, Nat. Commun. 6 (2015) 1–8, https://doi.org/10.1038/ncomms7883.

[15] L. Wang, K. Asheim, P.E. Vullum, A.M. Svensson, F. Vullum-Bruer, Sponge-like porous manganese(II,III) oxide as a highly efficient cathode material for rechargeable magnesium ion batteries, Chem. Mater. 28 (2016) 6459–6470, https://doi.org/10.1021/acs.chemmater.6b01016.

[16] P. Canepa, G. Sai Gautam, D.C. Hannah, R. Malik, M. Liu, K.G. Gallagher, K.A. Persson, G. Ceder, Odyssey of multivalent cathode materials: open questions and future challenges, Chem. Rev. 117 (2017) 4287–4341, https://doi.org/10.1021/acs.chemrev.6b00614.

[17] N. Sa, H. Wang, D.L. Proffit, A.L. Lipson, B. Key, M. Liu, Z. Feng, T.T. Fister, Y. Ren, C.-J.J. Sun, J.T. Vaughey, P.A. Fenter, K.A. Persson, A.K. Burrell, Is alpha-V$_2$O$_5$ a cathode material for Mg insertion batteries? J. Power Sources 323 (2016) 44–50, https://doi.org/10.1016/j.jpowsour.2016.05.028.

[18] G. Sai Gautam, P. Canepa, W.D. Richards, R. Malik, G. Ceder, Role of structural H2O in intercalation electrodes: the case of Mg in nanocrystalline Xerogel-V$_2$O$_5$, Nano Lett. 16 (2016) 2426–2431, https://doi.org/10.1021/acs.nanolett.5b05273.

[19] A. Parija, D. Prendergast, S. Banerjee, Evaluation of multivalent cation insertion in single-and double- layered polymorphs of V$_2$O$_5$, ACS Appl. Mater. Interfaces 9 (2017) 23756–23765, https://doi.org/10.1021/acsami.7b05556.

[20] G.S. Gautam, P. Canepa, A. Abdellahi, A. Urban, R. Malik, G. Ceder, The intercalation phase diagram of Mg in V$_2$O$_5$ from first principles, Chem. Mater. 27 (2015) 3733–3742, https://doi.org/10.1021/acs.chemmater.5b00957.

[21] G.S. Gautam, P. Canepa, R. Malik, M. Liu, K. Persson, G. Ceder, First-principles evaluation of multi-valent cation insertion into orthorhombic V$_2$O$_5$, Chem. Commun. 51 (2015) 13619–13622, https://doi.org/10.1039/C5CC04947D.

[22] B. Zhou, H. Shi, R. Cao, X. Zhang, Z. Jiang, Theoretical study on the initial stage of a magnesium battery based on a V$_2$O$_5$ cathode, Phys. Chem. Chem. Phys. 16 (2014) 18578–18585, https://doi.org/10.1039/C4CP02230K.

[23] J.C. Bouloux, I. Milosevic, J. Galy, Les hypovanadates de magnésium MgVO$_3$ et MgV$_2$O$_5$. Structure cristalline de MgVO3, J. Solid State Chem. 16 (1976) 393–398, https://doi.org/10.1016/0022-4596(76)90056-6.

[24] G.A. Horrocks, A. Parija, L.R. De Jesus, L. Wangoh, S. Sallis, Y. Luo, J.L. Andrews, J. Jude, C. Jaye, D.A. Fischer, D. Prendergast, L.F.J. Piper, S. Banerjee, Mitigating cation diffusion limitations and intercalation-induced framework transitions in a 1D tunnel-structured polymorph of V$_2$O$_5$, Chem. Mater. 29 (2017) 10386–10397, https://doi.org/10.1021/acs.chemmater.7b03800 acs.chemmater.7b03800.

[25] M. Onoda, N. Nishiguchi, Crystal structure and spin gap state of CaV$_2$O$_5$, J. Solid State Chem. 127 (1996) 359–362, https://doi.org/10.1006/jssc.1996.0395.

[26] N.A. Chernova, M. Roppolo, A.C. Dillon, M.S. Whittingham, Layered vanadium and molybdenum oxides: batteries and electrochromics, J. Mater. Chem. 19 (2009) 2526–2552, https://doi.org/10.1039/b819629j.

[27] J. Yao, Y. Li, R.C. Massé, E. Uchaker, G. Cao, Revitalized interest in vanadium pentoxide as cathode material for lithium-ion batteries and beyond, Energy Storage Mater 11 (2018) 205–259, https://doi.org/10.1016/j.ensm.2017.10.014.

[28] D. Muller-Bouvet, R. Baddour-Hadjean, M. Tanabe, L.T.N. Huynh, M.L.P. Le, J.P. Pereira-Ramos, Electrochemically formed α'-NaV$_2$O$_5$: a new sodium intercalation compound, Electrochim. Acta 176 (2015) 586–593, https://doi.org/10.1016/j.electacta.2015.07.030.

[29] L. Sánchez, J.-P. Pereira-Ramos, Electrochemical insertion of magnesium in a mixed manganese–cobalt oxide, J. Mater. Chem. 7 (1997) 471–473, https://doi.org/10.1039/a605210j.

[30] P. Novak, V. Shklover, R. Nesper , Magnesium insertion in vanadium oxides: a structural study, Zeitschrift Fur Phys. Chemie. 185 (1994) 51–68, https://doi.org/10.1524/zpch.1994.185.

[31] W.H. Yu, D.Z. Wang, B. Zhu, S.J. Wang, L.X. Xue, Insertion of bi-valence cations Mg^{2+} and Zn^{2+} into V$_2$O$_5$, Solid State Commun. 61 (1987) 271–273, https://doi.org/10.1016/0038-1098(87)90295-X.

[32] J.P. Pereira-Ramos, R. Messina, J. Perichon, Electrochemical formation of a magnesium vanadium bronze Mg$_x$V$_2$O$_5$ in sulfone-based electrolytes at 150°C, J. Electroanal. Chem. 218 (1987) 241–249, https://doi.org/10.1016/0022-0728(87)87019-5.

[33] G. Gershinsky, H.D. Yoo, Y. Gofer, D. Aurbach, Electrochemical and spectroscopic analysis of Mg^{2+} intercalation into thin film electrodes of layered oxides: V$_2$O$_5$ and MoO$_3$, Langmuir 29 (2013) 10964–10972, https://doi.org/10.1021/la402391f.

[34] T.D. Gregory, R.J. Hoffman, R.C. Winterton, Nonaqueous electrochemistry of magnesium, J. Electrochem. Soc. 137 (1990) 775–780, https://doi.org/10.1149/1.2086553.

[35] V. Shklover, T. Haibach, F. Ried, R. Nesper, P. Novak, Crystal structure of the product of Mg 2 ½ insertion into V$_2$O$_5$ single crystals, J. Solid State Chem. 323 (1996) 317–323, https://doi.org/10.1006/jssc.1996.0186.

[36] L. Yu, X. Zhang, Electrochemical insertion of magnesium ions into V$_2$O$_5$ from aprotic electrolytes with varied water content, J. Colloid Interface Sci. 278 (2004) 160–165, https://doi.org/10.1016/j.jcis.2004.05.028.

[37] C. Drosos, C. Jia, S. Mathew, R.G. Palgrave, B. Moss, A. Kafizas, D. Vernardou, Aerosol-assisted chemical vapor deposition of V$_2$O$_5$ cathodes with high rate capabilities for magnesium-ion batteries, J. Power Sources 384 (2018) 355–359, https://doi.org/10.1016/j.jpowsour.2018.02.074.

[38] S.-B. Son, T. Gao, S.P. Harvey, K.X. Steirer, A. Stokes, A. Norman, C. Wang, A. Cresce, K. Xu, C. Ban, An artificial interphase enables reversible magnesium chemistry in carbonate electrolytes, Nat. Chem. 10 (2018) 532–539, https://doi.org/10.1038/s41557-018-0019-6.

[39] M. Hayashi, H. Arai, H. Ohtsuka, Y. Sakurai, Electrochemical insertion/extraction of calcium ions using crystalline vanadium oxide, Electrochem. Solid state Lett. 7 (2004) A119–A121, https://doi.org/10.1149/1.1675951.

[40] H. Wang, P. Senguttuvan, D.L. Proffit, B. Pan, C. Liao, A.K. Burrell, J.T. Vaughey, B. Key, Formation of MgO during chemical magnesiation of Mg-Ion battery materials, ECS Electrochem. Lett. 4 (2015) A90–A93, https://doi.org/10.1149/2.0051508eel.

[41] A. Mukherjee, N. Sa, P.J. Phillips, A. Burrell, J. Vaughey, R.F. Klie, Direct investigation of Mg intercalation into the orthorhombic V$_2$O$_5$ cathode using atomic-resolution transmission electron microscopy, Chem. Mater. 29 (2017) 2218–2226, https://doi.org/10.1021/acs.chemmater.6b05089.

[42] P. Novák, J. Desilvestro, Electrochemical insertion of magnesium in metal oxides and sulfides from aprotic electrolytes, J. Electrochem. Soc. 140 (1993) 140–144, https://doi.org/10.1149/1.2056075.

[43] S.C. Lim, J. Lee, H.H. Kwak, J.W. Heo, M.S. Chae, D. Ahn, Y.H. Jang, H. Lee, S.T. Hong, Unraveling the magnesium-ion intercalation mechanism in vanadium pentoxide in a wet organic electrolyte by structural determination, Inorg. Chem. 56 (2017) 7668–7678 https://doi.org/10.1021/acs.inorgchem.7b00204.

[44] A. Yoshikawa, K. Yagisawa, M. Shimoda, Crystal structure and hydrogen occupation in H$_x$V$_2$O$_5$ (x = 0.0-3.9), J. Mater. Process. Technol. 29 (1994) 1319–1323, https://doi.org/10.1007/BF00975082.

[45] H.T. Evans, M.E. Mrose, The crystal structures of three new vanadium oxide minerals, Acta Crystallogr. 11 (1958) 56–58, https://doi.org/10.1107/S0365110X58000141.

[46] H.T. Evans, M.E. Mrose, A crystal chemical study of the vanadium oxide crystals, Häggite and Doloresite, Am. Mineral. 45 (1960) 1144–1165.

[47] V.C. Srivastava, S. Gupta, K.N. Rai, J. Kumar, Hydrogen absorption in vanadium pentoxide, Mater. Res. Bull. 23 (1988) 341–348, https://doi.org/10.1016/0025-5408(88)90007-4.

[48] M. Cabello, F. Nacimiento, J.R. González, G. Ortiz, R. Alcántara, P. Lavela, C. Pérez-Vicente, J.L. Tirado, Advancing towards a veritable calcium-ion battery: CaCo$_2$O$_4$positive electrode material, Electrochem. Commun. Now. 67 (2016) 59–64, https://doi.org/10.1016/j.elecom.2016.03.016.

[49] H.K. Lim, Y.S. Choi, S.T. Hong, Magnesium perchlorate anhydrate, Mg(ClO$_4$)$_2$, from laboratory X-ray powder data, Acta Crystallogr. Sect. C Cryst. Struct. Commun. 67 (2011) 36–38, https://doi.org/10.1107/S0108270111015861.

[50] R.J.D. Tilley, B.G. Hyde, An electron microscopic investigation of the decomposition of V$_2$O$_5$, J. Phys. Chem. Solid. 31 (1970) 1613–1619, https://doi.org/10.1016/0022-3697(70)90045-4.

[51] R. Enjalbert, J. Galy, A refinement of the structure of V$_2$O$_5$, Acta Crystallogr. 42 (1986) 1467–1469, https://doi.org/10.1524/zkri.1971.133.133.75.

On the strange case of divalent ions intercalation in V_2O_5

R. Verrelli, A.P. Black, C. Pattanathummasid, D. Tchitchekova, A. Ponrouch, J. Oro-Sole, C. Frontera, F. Barde, P. Rozier, M.R. Palacin

Supporting Information
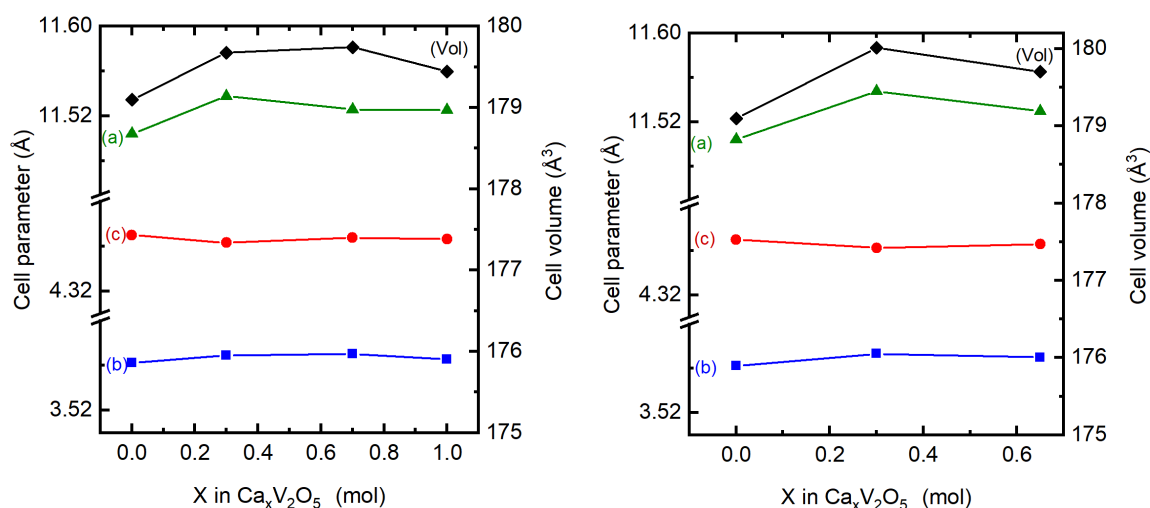
S 1. Cell parameters and cell volume against Δx mols inserted at different stages of galvanostatic reduction of V_2O_5 tape electrodes in Ca cells (A) in $Ca(BF_4)_2$, (B) in $Ca(TFSI)_2$ in EC:PC 1:1v electrolites.

α-V_2O_5	OCP	1st Reduction	1st Oxidation
		(140 mAh g^{-1})	
Radiation	X-ray Mo $k_{\alpha 1}$	X-ray Mo $k_{\alpha 1}$	X-ray Mo $k_{\alpha 1}$
System	Orthorhombic	Orthorhombic	Orthorhombic
Space group	*Pmmn*	*Pmmn*	*Pmmn*
a (Å)	11.517(4)	11.540(2)	11.520(2)
b (Å)	3.568(1)	3.5697(4)	3.5624(1)
c (Å)	4.366(2)	4.3703(6)	4.3711(1)
β (º)	90.0	90.0	90.0

Table S1: Crystallographic data refined for V_2O_5 tape electrode after OCP, partial reduction (120 mAh g^{-1}) and after re-oxidation in 0.3 M $Mg(ClO_4)_2$ EC:PC (1:1 v) electrolyte.

α- V$_2$O$_5$	H$_6$V$_4$O$_{10}$
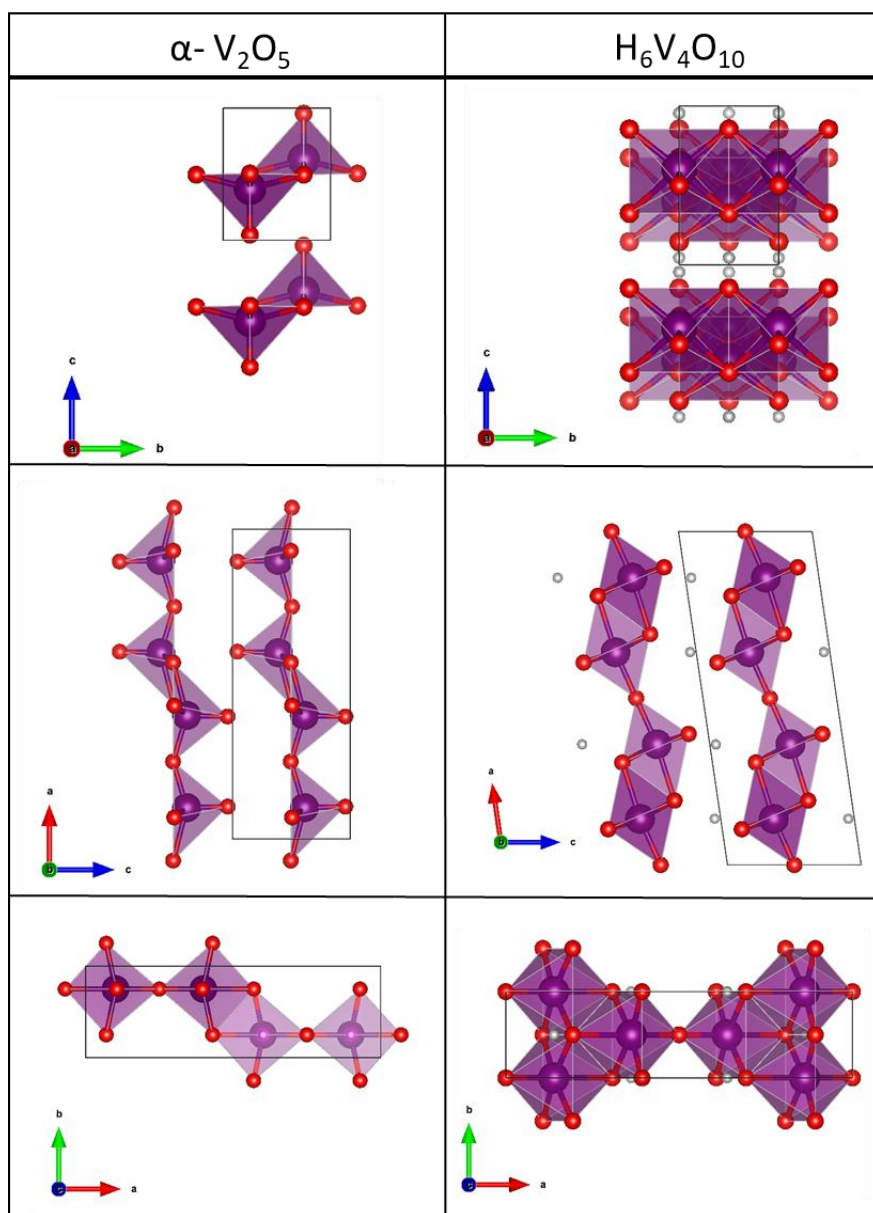
S 2. Structural model of α-V$_2$O$_5$ and Häggite (H$_6$V$_4$O$_{10}$) showing projections along a, b and c axis. Vanadium is represented in purple, oxygen in red and hydrogen in grey.
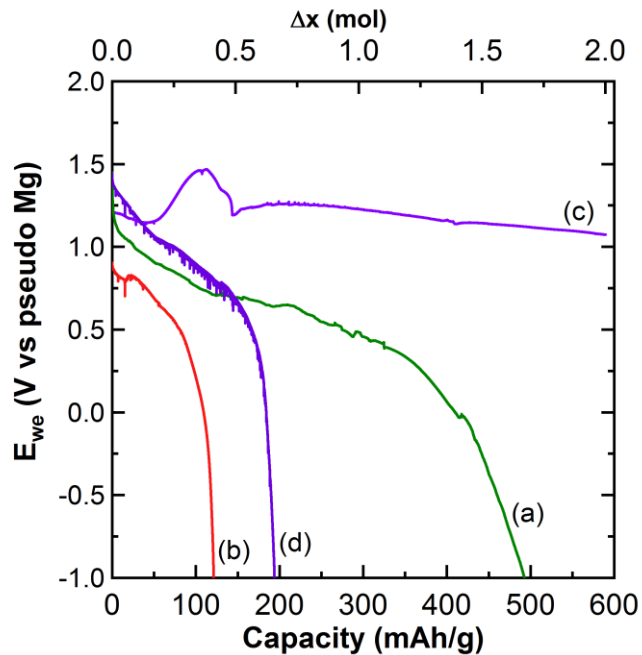
(A)
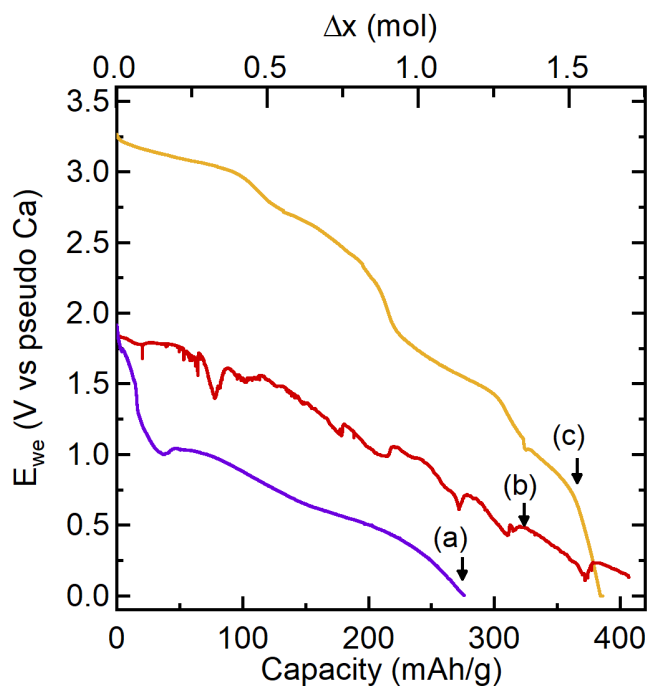
(B)

*S 3. Characteristic GCPL voltage profile versus specific capacity (bottom axes) and versus moles of inserted ion (Δx) (top axis), considering that all electrochemical response is related to divalent ion intercalation in V₂O₅, in Mg **(A)** and Ca **(B)** cells employing wet electrolytes. C/100 rate. (A): (a) 0.5 M Mg(ClO₄)₂, ACN + 1 M H₂O, RT, (b) 0.3 M Mg(TFSI))₂, EC:PC + 1M H₂O, RT, (c) 0.3 M Mg(ClO₄)₂, EC:PC + 1M H₂O, RT, (d) 0.3 M Mg(ClO₄)₂, EC:PC + 1M H₂O, 100°C. (B): (a) Ca/0.3 M Ca(ClO₄)₂, EC:PC 1:1 v + 0.3M H₂O,100°C ,(c) 0.3 M Ca(TFSI)₂, EC:PC 1:1 v + 0.3M H₂O, 100°C , (d) Ca/1 M Ca(BF₄)₂, EC:PC 1:1 v + 0.3M H₂O, 100°C.*

Open circuit potential (OCP)
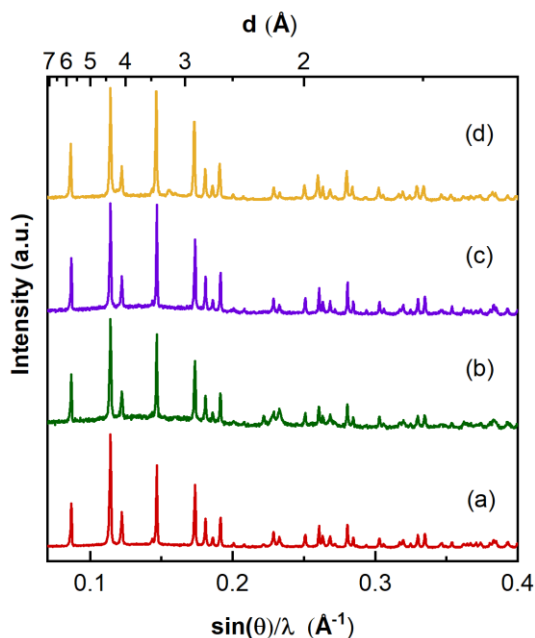
S4. XRD patterns of V_2O_5 electrodes left for 4 days at OCP at RT in various electrolytes. (a) 0.3M Ca(TFSI)$_2$ /EC:PC, (b) 1M Ca(ClO$_4$)$_2$ /ACN , (c) 0.3M Ca(ClO$_4$)$_2$ /EC:PC, (d) 1M Ca(BF$_4$)$_2$ /EC:PC.

V_2O_5 Chemical Stability
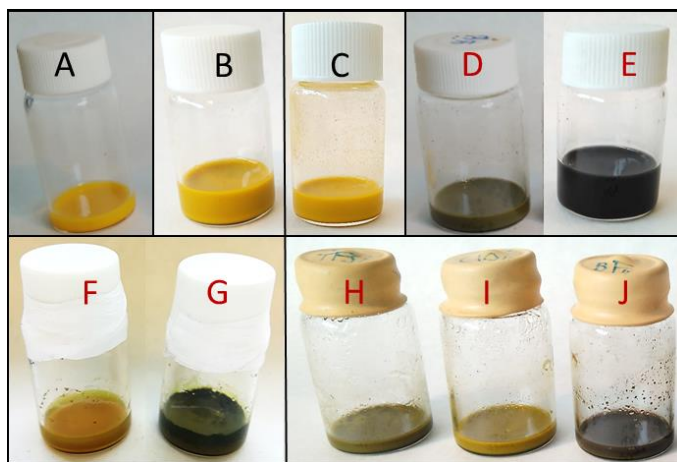
S 5. Images of V_2O_5 chemical stability in bare carbonate solvents and in various electrolyte solutions. A) pristine V_2O_5 in EC:PC at t=0 at RT. B) V_2O_5 in EC:PC after 1 week at RT. C) V_2O_5 in ACN after 1 week at RT. D) V_2O_5 in EC:PC after 1 week at 100°C. E) V_2O_5 in EC:PC after 1 month at 100°C. F) V_2O_5 in Mg(ClO$_4$)$_2$ /EC:PC after 1 week at 100°C. G) V_2O_5 in Mg(TFSI)$_2$ /EC:PC after 1 week at 100°C. H) V_2O_5 in Ca(TFSI)$_2$ /EC:PC after 1 week at 100°C. I) V_2O_5 in Ca(ClO$_4$)$_2$ /EC:PC after 1 week at 100°C. J) V_2O_5 in Ca(BF$_4$)$_2$ /EC:PC after 1 week at 100°C.
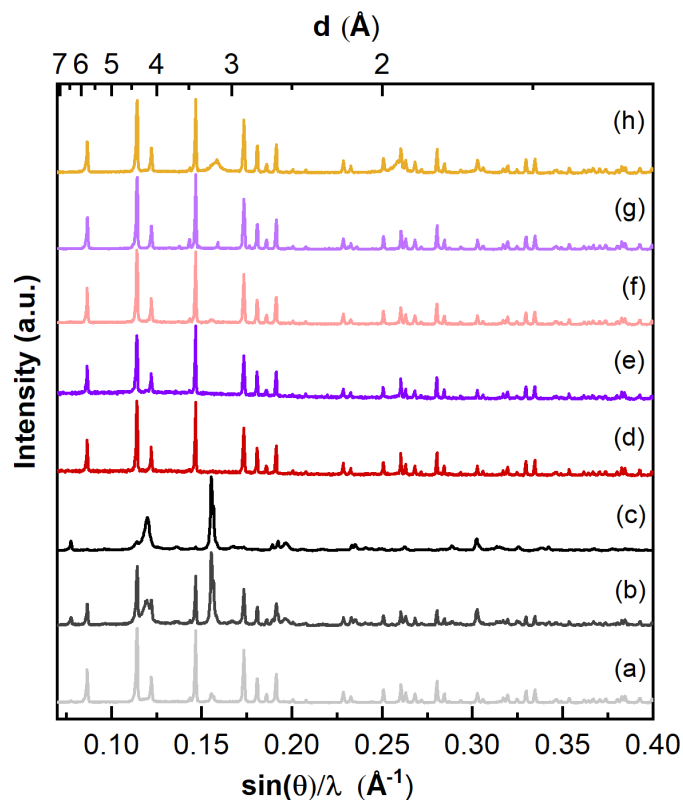
S 6. XRD patterns of (a) V_2O_5 in EC:PC after 1 week at 100°C, (b) V_2O_5 in EC: PC after 1 month at 100°C, (c) V_2O_5 in EC:PC after 6 weeks at 100°C, (d) V_2O_5 in $Mg(TFSI)_2$ /EC:PC after 1 week at 100°C, (e) V_2O_5 in $Mg(ClO_4)_2$ /EC:PC after 1 week at 100°C. (f) V_2O_5 in $Ca(TFSI)_2$ /EC:PC after 1 week at 100°C. (g) V_2O_5 in $Ca(ClO_4)_2$ /EC:PC after 1 week at 100°C. (h) V_2O_5 in $Ca(BF_4)_2$ /EC:PC after 1 week at 100°C.
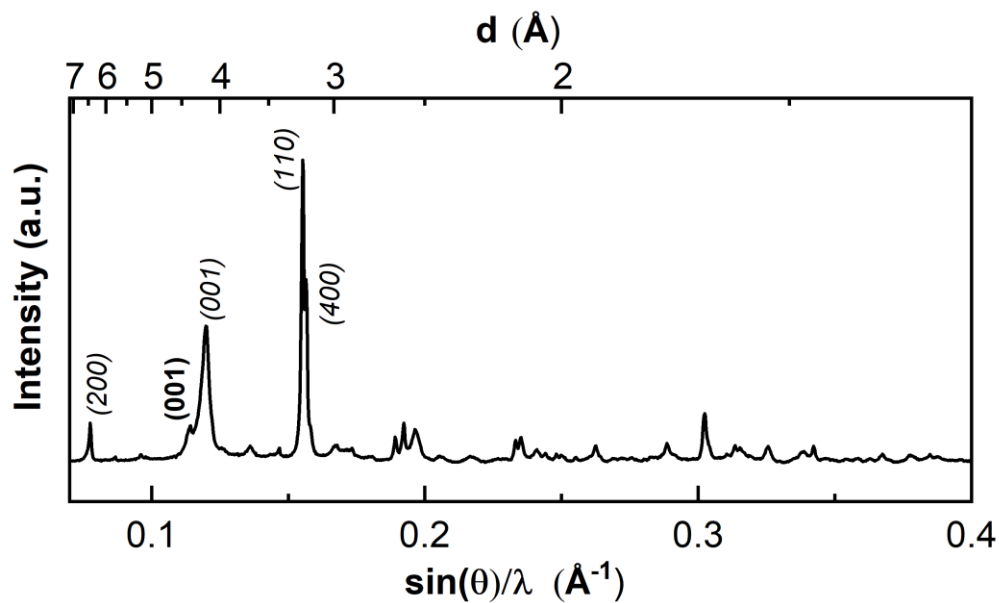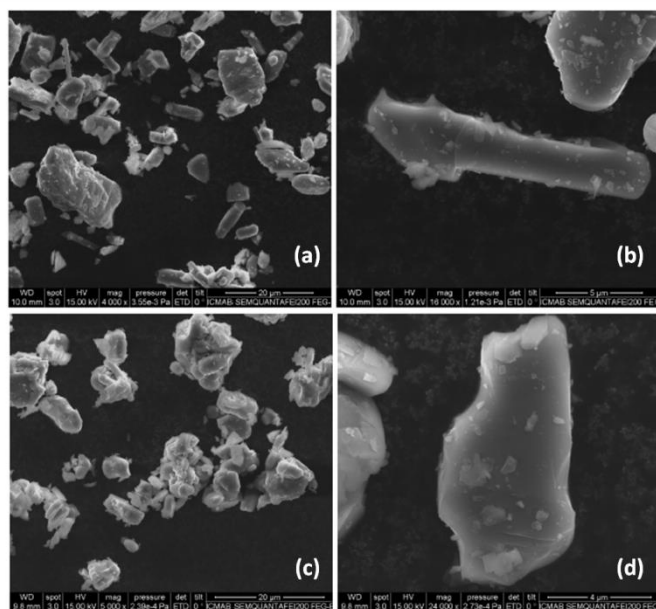

S 7. XRD patterns of V_2O_5 in EC:PC after 6 weeks at 100°C. Indexing of main reflections in italic for Orthorhombic γ-$H_xV_{2-x}O_5(VO_x)$ and in bold α-V_2O_5.
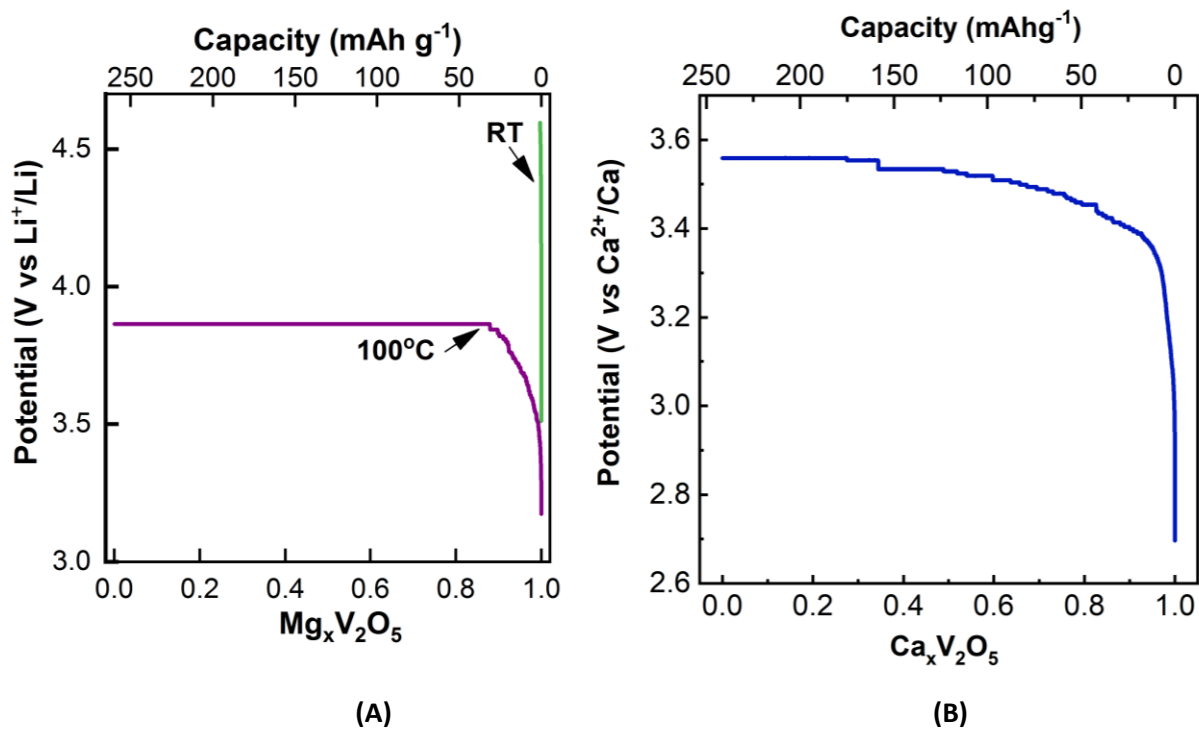
AV₂O₅ (A= Mg, Ca)
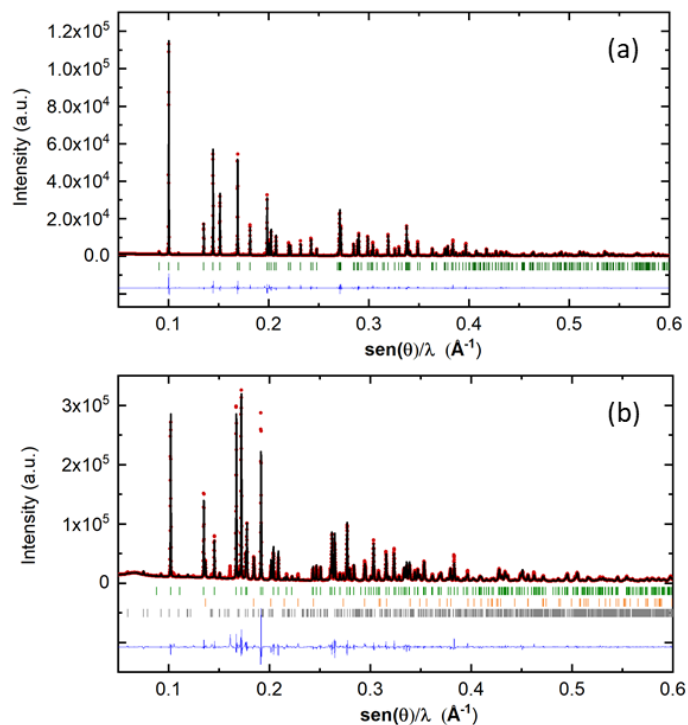
(A)

(B)

S8. (A) Observed and calculated synchrotron X-ray powder diffraction patterns at room temperature for (a) MgV₂O₅ and (b) CaV₂O₅. Impurities of V₂O₃ (orange ticks) and Ca₃V₂O₈ (black ticks); (B) SEM micrographs of the MgV₂O₅ sample prepared by direct synthesis [(a)-(b)] and comproportionation [(c)-(d)].

S9. Characteristic Voltage-composition profile of the MgV$_2$O$_5$ electrode at RT (green curve) and 100°C (purple curve) (a) and of the CaV$_2$O$_5$ electrode at 100°C (b). The bottom scale (Δx) corresponds to moles of intercalated ion considering that all electrochemical response is related to divalent ion intercalation in V$_2$O$_{5,}$